Lamellae tungsten tile design transient thermal/ electromagnetic stress analysis

Thomas Willard*, Rui Vieira, Samuel Pierson
MIT Plasma Science and Fusion Center,
Cambridge, MA 02139

8 June 2006

Abstract

A transient thermal/ electromagnetic stress analysis of the lamellae tungsten tile design has been performed to determine if the design is adequate to meet the maximum design load conditions of 12 MW/ m^2 uniform heat flux for 5 seconds (single pulse, no Diverter Plate temperature ratcheting) , superimposed on the electromagnetic body load due to eddy currents generated by disruptions. The results show that the design is adequate, with the stresses in the tungsten lamellae and the TZM molybdenum hardware less than the ultimate strength of the materials at temperature.

Scope

This memo documents the analysis of the final version of the lamellae tungsten tile design. Earlier interim designs, using swaged rivets, D-cross section shoulder screws, or square-cornered screw heads (some tested in the High Heat Flux (HHF) e-beam test facilities at Sandia and Juerlich) are not included.

1. Introduction

The plasma-facing surfaces of the mono-block TZM molybdenum tiles presently lining the Lower Diverter plates show evidence of melting and cracking (Fig.1.1), due to the high heat flux from contact with the plasma, and the large electromagnetic body loads from disruptions.

An upgrade design has been developed to extend the operating pulse-on time rating of the tiles from the present 1-2 seconds to 5 seconds, to better resist melting, and to prevent cracking from disruptions.

The new design uses a tungsten (W) lamellae construction to reduce the eddy currents generated by disruptions: the electrical contact resistance between the lamella reduces the currents that would exist in a solid, mono-block design.

Tungsten was chosen for the lamella material over molybdenum due to its higher melting temperature (3400 C vs 2600 C).

2. Model Description

Note: The finite element analysis below was performed using ANSYS Multiphysics 10.0 software. The solid models used in the analysis were created using SolidEdge v 17.

Detail drawings for the tile assembly and all of its components are shown in Appendix A.

As shown in the drawings, the design consists of a stack of eight 4mm thick tungsten lamella, held together with a TZM molybdenum #1/4-28 shoulder screw and nut.

Countersunk holes in the endplates and radiused heads on the screw and the nut create line contact between the components, minimizing heat conduction and preventing any bending moment from transferring to the screw.

The cross section of the shoulder screw is wedge shaped to create area contact between the screw and the mating angled surface of the thru-hole in the lamellae. This allows the temperature of the screw to more closely match the local (hole centerline) temperature of the lamellae, so the screw can expand at the same rate, reducing the stresses both in the screw and the lamellae.

The tile assembly mounts to the 304L stainless steel Diverter Plate using a #10-32 TZM molybdenum cap screw and a stack of two Inconel 718 Belleville washers, located under the head of the cap screw to allow for the large difference in coefficient of expansion (CTE) between the screw and the Diverter Plate.

A slot in the base of the lamellae reduce the thermal stresses due to the difference in expansion, top-to-bottom, from the large thermal gradient in the lamellae.

2.1 Solid Model Geometry

The full solid model, constructed from the detailed drawings in Appendix A, is shown in Fig. 2.1.1. In addition to the tile assembly itself, a section of the 304L stainless steel Diverter Plate on which the tile is mounted is included in the model. Note: The expansion slot, machined in the base of the lamellae to reduce the thermal stresses, are highlighted in the figure.

It is seen from Fig. 2.1.1 that a plane of symmetry exists in the model, coinciding with the axis of the shoulder screw. Therefore, to save computation time, the half solid model shown in Fig. 2.1.2 was used in the analysis.

Note: The Inconel 718 Belleville washers (Fig. 2.1.2) used under the head of the TZM mounting cap screw are .394" O.D., .206" I.D., .027" thick, and are available from Key Belleville, Inc., P/N 1-5.3-.7-718. The spring rate of the washer is 2.39E04 lbf/in.

2.2 Material Properties

The sintered powder metal (PM) tungsten sheet used in the design is from PLANSEE, and is made to their

material specification 39.30.31 GF016 part 7E, rev 5. The material is provided hot rolled and fully annealed.

The PM TZM molybdenum rod used in the design is also from PLANSEE (material specification 39.20.40-GR101 part 7E, rev. 5), and is also hot rolled and fully annealed.

All the material mechanical and thermal properties used in the analysis, along with the source references, are listed in Tables 2.2.1 and 2.2.2.

The stress-strain vs. temperature curves for annealed TZM rod from Ref. [4] are shown in Fig. 2.2.1.

The ultimate strength vs. temperature curves for tungsten sheet for several material conditions (blue curve condition similar to PLANSEE sheet) from Ref. [5] are shown in Fig. 2.2.2 . The very high temperature ultimate and yield strength curves for PLANSEE sheet (1mm thick) from Ref. [6] are shown in Fig. 2.2.3. Crack heat flux vs. temperature and number of cycles for tungsten sheet for several material conditions (W-PM condition similar to PLANSEE sheet) from Ref. [7] are shown in Fig. 2.2.4.

Combining the curves from the above references, the yield and ultimate strength vs. temperature curves used to evaluate the results of the analysis are shown in Fig. 2.2.5.

2.3 Contact

2.3.1 Mechanical Contact

The mechanical contact used at each joint in the model are shown in Fig. 2.3.1.

Frictionless contact was used to allow sliding between the lamellae and between the base of the lamellae and the Diverter Plate.

To prevent relative motion between mated thread parts (see Figures 2.1.2 and 2.3.1), bonded contact was used between the threaded section of the TZM cap screw and the TZM shoulder screw. Bonded contact was also used to join the threaded and unthreaded sections of the screws, divided in the solid model to permit application of the pre-tension loads.

With the large amount of frictionless contact in the model, convergence was an issue. To prevent rigid body motion and to improve convergence, rough contact (no sliding) was used between the head of the cap screw and the Diverter Plate. The normal stiffness factor of the joint was also changed to 9.0E-04 (determined in a separate FEA model not included here) to simulate the stiffness of the Belleville washer stack .

2.3.2 Thermal Contact

The material combinations at each joint in the model, used to determine the thermal contact conductance at the joints, are shown in Fig. 2.3.1.

From Ref. [8-10], for conforming (flat) rough surfaces in a vacuum, the thermal conductance at a joint is a function of: 1.) the thermal

conductivity of the materials (function of temperature); 2.) the contact pressure; 3.) the roughness of the surfaces; 4.) the hardness of the surfaces (function of temperature); and the vacuum pressure.

A survey of the literature produced no published measured data for the combination of materials, temperatures, surface roughness, and contact pressure present in the design.

The thermal conductances used in the model were determined using the equations from Ref. [8-10], along with the thermal properties data from Table 2.2.2, and the surface finishes specified on the drawings in Appendix A. Note: The initial average contact pressure at each joint, required to determine the conductance, was calculated assuming a preload on both the shoulder screw and cap screw of 250 lbf (half compression of the Belleville washer stack).

An example calculation for the W-TZM joint combination is included in Appendix B. The calculated thermal contact conductances for all the material joint combinations used in the model are listed in Table 2.3.1.

Note: The thermal conductance values used in the model have a great effect on the calculated temperature profile and the resulting thermal stresses.

To accurately determine the thermal stresses, the conductance values must be known to within a factor of 3 or better. Since no published measured values have been found, and experience with calculated values from Ref. [8-10] is limited for refractory materials in vacuum at high temperature, an in-house thermal contact resistance test facility is being built, to the requirements of Ref. [11-13], to verify the calculated values used in the model.

2.4 Mesh

The mesh used in the analysis is shown in Fig. 2.4.1. The ANSYS automatically generated mesh (shape checking controls on) consists of 431272 nodes and 284700 elements (SOLID 187, tetrahedron). Note: A model with half the mesh density showed no significant difference in results.

2.5 Boundary Conditions

2.5.1 Thermal Model

The boundary conditions used for the nonlinear (radiation) transient thermal analysis are shown in Fig. 2.5.1.

The plasma-facing surface has a uniform applied heat flux of 1200 W/ cm^2 [14], and radiates to an ambient of 22 C. The surface emissivity is .25 (tungsten [15]).

The base/ underside of the Diverter Plate radiates to an ambient of 22 C, and has a surface emissivity of .5 (304L [3]).

The uniform initial temperature is 22 C, and the pulse length is 5 seconds. Note: This analysis is for a single

pulse, and does not include the effect of Diverter Plate temperature ratcheting with a series for pulses.

2.5.2 Thermal Stress Model

The boundary conditions used for the nonlinear (contact) thermal stress analysis are shown in Fig. 2.5.2.

The nodal temperatures are from the last time step (5 seconds) of the previous transient thermal analysis.

The faces on the symmetry plane are constrained from moving in the Z (plane of symmetry) direction.

The face of the Diverter Plate base/ underside is constrained from moving in the X (radial) direction.

The broad face of the center lamellae is constrained from moving in the Y (circumferential) direction.

Note: The expansion joints used to mount the Diverter Plate in the vessel allow expansion in the circumferential direction, but not in the radial direction. Also, for the large diameter vessel, the curvature of the Diverter Plate is assumed to be zero.

A pre-tension load of 125 lbf (250 lbf for a full screw) is applied to the halves of both the shoulder screw and the cap screw.

2.5.3 Thermal Stress+ Emag Model

The boundary conditions used for the nonlinear thermal stress + Emag analysis are shown in Fig. 2.5.3.

The boundary conditions are the same as for the previous thermal stress analysis (see Fig. 2.5.2), with the addition of the opposing pressure loads applied to the plasma-facing surfaces of the two end plates, equivalent to the electromagnetic loads generated by disruptions.

Note: The disruption event used here is defined in Ref. [16] as the collapse of a 1 Tesla poloidal field in 3 milliseconds crossed with a static 7 Tesla toroidal field.

This equivalent pressure load was determined by a separate, simplified finite element model and hand analysis based on the procedure outlined in Ref. [16] which are included in Appendix C.

Note: The electrical conductance ratio β used in Ref. [16] and the analysis in Appendix C is the ratio of the bulk material conductance (isotropic) to the effective conductance in the direction across the interface of the lamellae, reduced for the electrical contact resistance between the mating surfaces (orthotropic).

Like thermal contact resistance, the electrical contact resistance is a function of the contact pressure and also the temperature, roughness, flatness, and electrical conductivity of the two surfaces. A survey of the literature produced no published measured data for the electrical contact resistance of W-W, W-TZM, or W-304L joints. Since no published data was available, electrical contact resistance measurements were

made in-house [17] and used in the electromagnetic load analysis in Appendix C.

3. Results

3.1 Temperature Profile

The temperature profile at the end of the 5 second time step is shown in Fig. 3.1.1. The transient response of the highest temperature node is also shown in the figure.

The results show that the highest temperature reached by the plasma-facing W surface is 1914 C.

3.2 Thermal Stress Profile

The overall thermal stress profile at the end of the 5 second pulse is shown in Fig. 3.2.1. As shown in the figure, the maximum stress/ highest temperature combination on the plasma-facing surfaces of the W lamellae is 16042 psi at 1840 C. From the strength vs. temperature curves of Fig. 2.2.5, the stress is at the ultimate strength limit of the tungsten. This will be discussed further below (see Section 4. Conclusions).

Note: The high stress areas in the 304L stainless steel Diverter Plate section of Fig. 3.2.1 are in excess of the high temperature strength rating of the steel [3]. It is recognized that the Diverter Plate and its expansion joint mounts must be redesigned to match the increased power rating of the tiles, but their redesign is beyond the scope of the present effort. For this analysis, the high stress areas in the stainless steel will be ignored.

Fig. 3.2.2 is an overall side view showing the Y axis (circumferential) deformation. Fig. 3.2.3 shows the X-axis (radial) deformation. From the two figures, it can be seen that the plasma-facing surface of the lamellae expands much more than the base surface, causing the faces of the endplates to rotate relative to the shoulder screw and nut. The radiused contact faces on the screw and nut allow only line contact and prevent the rotation of the endplates from applying a bending moment to the screw, as shown by the lack of bending of the screw in the figures.

Fig. 3.2.4 shows the thermal stress profile in the W lamella shoulder-nut endplate. From the figure, the maximum stress/ highest temperature combination is 23754 psi at 1601 C, and occurs in the 60° countersunk face area along the line of contact with the shoulder nut. From Fig. 2.2.5, this stress is at or slightly below the ultimate strength of the tungsten. However, the stress is extremely localized, and is a Hertzian contact/ bearing stress (compressive). For most materials, the strength in bearing is 2-3 times higher than that from simple tension tests. Therefore, this stress is not considered to be excessive.

Fig. 3.2.5 shows the thermal stress profile in the W lamella shoulder-screwhead endplate. From the figure, the maximum stress/ highest temperature combination is 25466 psi at 1550 C and occurs in the 60° countersunk area along the line of contact with the shoulder screw. From Fig. 2.2.5, this stress is slightly below the ultimate strength of the

tungsten, and is also a bearing stress, and is not considered to be excessive.

Figures 3.2.6 and 3.2.7 show the thermal stress profile in the TZM shoulder screw and nut and the cap screw. From the figures, the maximum stress/ highest temperature combination is 116250 psi at 380 C and occurs in the shoulder screw, at the root of the #1/4-28 threads. From Fig. 2.2.5, this stress is above the ultimate strength of the TZM. However, this highly localized stress is the result of a singularity/ sharp edge in the model, and can easily be reduced by radiusing the edge. Even a .015"' radius, a typical machining 'sharp' corner radii minimum value, will greatly reduce this stress.

3.3 Thermal Stress + Emag Profile

Fig. 3.3.1 shows the overall stress profile for the combined thermal and electromagnetic (Emag) load condition. A comparison with Fig. 3.2.1 (thermal stress only), shows that the electromagnetic load adds little or no additional stress.

3.4 Minimum Emag Tipping Load

The lamellae of the tile assembly are held to the Diverter Plate by the 250 lbf (minimum) pre-tensioned cap screw, resulting in a uniform pressure on the mating wedge-shaped faces of the shoulder screw and lamellae. The minimum electromagnetic load required to overcome this force and produce tipping or rocking of a single lamellae was calculated by hand (see Appendix D) and the results are shown in the free body diagram of Fig. 3.4.1. The required tipping load of 15.6 lbf is approximately three times the calculated electromagnetic load from disruption, so tipping should not occur.

4. Conclusions

The design limit condition, where the maximum stress/ highest temperature combination exists, occurs on the plasma-facing surfaces of the W lamellae: 16042 psi at 1840 C. From the strength vs. temperature curves of Fig. 2.2.5, this stress is at or slightly above the ultimate strength of the tungsten, which would normally mean the design is inadequate.

However, several factors tend to make this assessment conservative: 1.) the 12 MW/m^2 uniform heat flux , applied in the model as a square pulse, actually has a ~ half second rise and fall time that reduces the total input energy, which should result in lower temperatures and thermal stresses; 2.) recent e-beam melt spot tests from Ref. [18] (1.5 GW/m^2 for 3 seconds applied to a Ø1mm area) on free-standing PLANSEE W-sheet produced no macro-cracking in the sheet; 3.) crack formation vs heat flux and number of cycles tests from Ref. [7] (see Fig. 2.4.4) on free-standing W-sheet showed no crack propagation after 1000 cycles at 35 MW/m^2 ; and 4.) the high stress is located in a non-structural area where cracking, if it occurs, will not cause catastrophic failure of the tile assembly.

For the above reasons, the present W-lamellae tile design is considered to be adequate to meet the maximum design load conditions of 12 MW/ m^2 uniform heat flux for 5 seconds (single pulse, no Diverter Plate temperature ratcheting). It is recommended, though, that a full power test of the assembly be performed to verify the above results.

References:

[1] MatWeb.com Online Materials Database, "Tungsten, W".

[2] ASM International Alloy Digest, "TZM High Temperature Molybdenum Alloy", 1964.

[3] Allegheny Ludlum Technical Data Sheet, "Stainless Steel Types 302, 304, 304L, 305", (1998) 1-9.

[4] ASM International Atlas of Stress-Strain Curves, "TZM molybdenum alloy rolled rounds, tensile stress-strain curves at room and elevated temperatures", (2002)

[5] M. Greiger et al., "Structure and mechanical properties of formed tungsten based materials", *J. Materials Processing Technology* Vol. 157–158 (2004) 683–687

[6] B. Fischer et al., "Creep and tensile tests on refractory metals at extremely high temperatures", *International J. Refractory Metals & Hard Materials* Vol. 24 (2006) 292–297

[7] X. Liu et al., "High heat flux properties of pure tungsten and plasma sprayed tungsten coating**",** *J. Nuclear Materials* Vol. 329–333 (2004) 687–691

[8] M. Bahrami et al, "Review of thermal joint resistance models for non-conforming rough surfaces in a vacuum", *Proc. HTC'03, ASME Summer Heat Transfer Conf.* HT2003-47051 (2003) July 21-23, Las Vegas, NV

[9] S. Song et al, "Relative contact pressure: Dependence on surface roughness and Vickers microhardness", *J. Thermophysics* Vol. 2, No. 1 (1988) 43-47.

[10] I. Savija et al, "Review of thermal conductance models for joints incorporating enhancement materials", AIAA-2002-00494*.*

[11] J. R. Culham et al, "Design, assembly, and commissioning of a test apparatus for characterizing thermal interface materials", *IEEE Inter. Society Conf. on Thermal Performance* (2002)

[12] I. Savija et al, "Effective thermophysical properties of thermal interface materials: Part I Definitions and models", *Proc. IPACK03, Int. Electronic Packaging Tech. Conf. and Exhibit.* IPACK2003-35088 (2003) July 6-11, Maui, Hawaii

[13] "Standard test method for thermal transmission properties of thin thermally conductive solid electrical insulation material", *ASTM D 5470-01*

[14] G. Loesser et al, "Memorandum of Understanding: Collaboration

agreement MIT and PPPL for lower hybrid coupler current drive launcher", MOU-MIT-PPPL-1100, 6 December 2000

[15] "Tungsten emissivity", *ITER Materials Properties Handbook, Boeing High Energy Systems*

[16] B. Lipshultz, "Estimate of the forces on a W lamellae tile", *MIT Plasma Science and Fusion Center,* 15 July 2005

[17] S. Pierson, "Tungsten lamellae tile electrical contact resistance test results", *MIT Plasma Science and Fusion Center*, 23 May 2006

[18] S. Pierson, "Lamellae W-tile e-beam spot melt test**",** *MIT Plasma Science and Fusion Center,* 25 April 2006

Table 2.2.1 - Material Mechanical Properties

Material	Young's Modulus		Poisson's Ratio	CTE		Brinell Hardness	
	(lbm/ in^2)	(MPa)		(1/ F)	(1/ C)	(kgf/mm^2)	(GPa)
W- Tungsten [1]	5.900E+07	4.068E+05	0.28	2.444E-06	4.400E-06	294	2.88
TZM - Molybdenum [2]	4.600E+07	3.172E+05	0.321	3.444E-06	6.199E-06	217	2.13
304L - Stainless Steel [3]	2.900E+07	2.000E+05	0.30	1.111E-05	2.000E-05	201	1.97

Table 2.2.2 - Material Thermal Properties

Material	Density		Thermal Conductivity		Specific Heat	
	(lbm/ in^3)	(g/ cm^3)	(BTU/ s in F)	(W/ m K)	(BTU/ lbm F)	(J/ kg K)
W- Tungsten [1]	0.696	19.25	2.180E-03	163	3.198E-02	134.0
TZM - Molybdenum [2]	0.369	10.21	1.759E-03	131.54	6.000E-02	251.4
304L - Stainless Steel [3]	0.284	7.85	2.176E-04	16.269	0.120	502.8

Table 2.3.1 - Thermal Contact Conductances

Joint Materials	Surface Finishes (uin RMS)	Contact Area A (in^2)	Initial Contact Pressure [(1)] P (psi)	Contact Conductance h	
				(BTU/s in^2 R)	(W/m^2 K)
W-W	125-125	0.749	334	2.806E-03	8.261E+03
W-TZM	32- 64	0.312	402[(2)]	4.767E-03	1.403E+04
W-304	64- 32	1.200	208	5.144E-04	1.514E+03

Note:
1. Initial contact pressure based on bolt preload of 250 lbf: P=250/A.
2. Contact pressure on 60 degree angled wedge faces: P=250/A *sin 30.

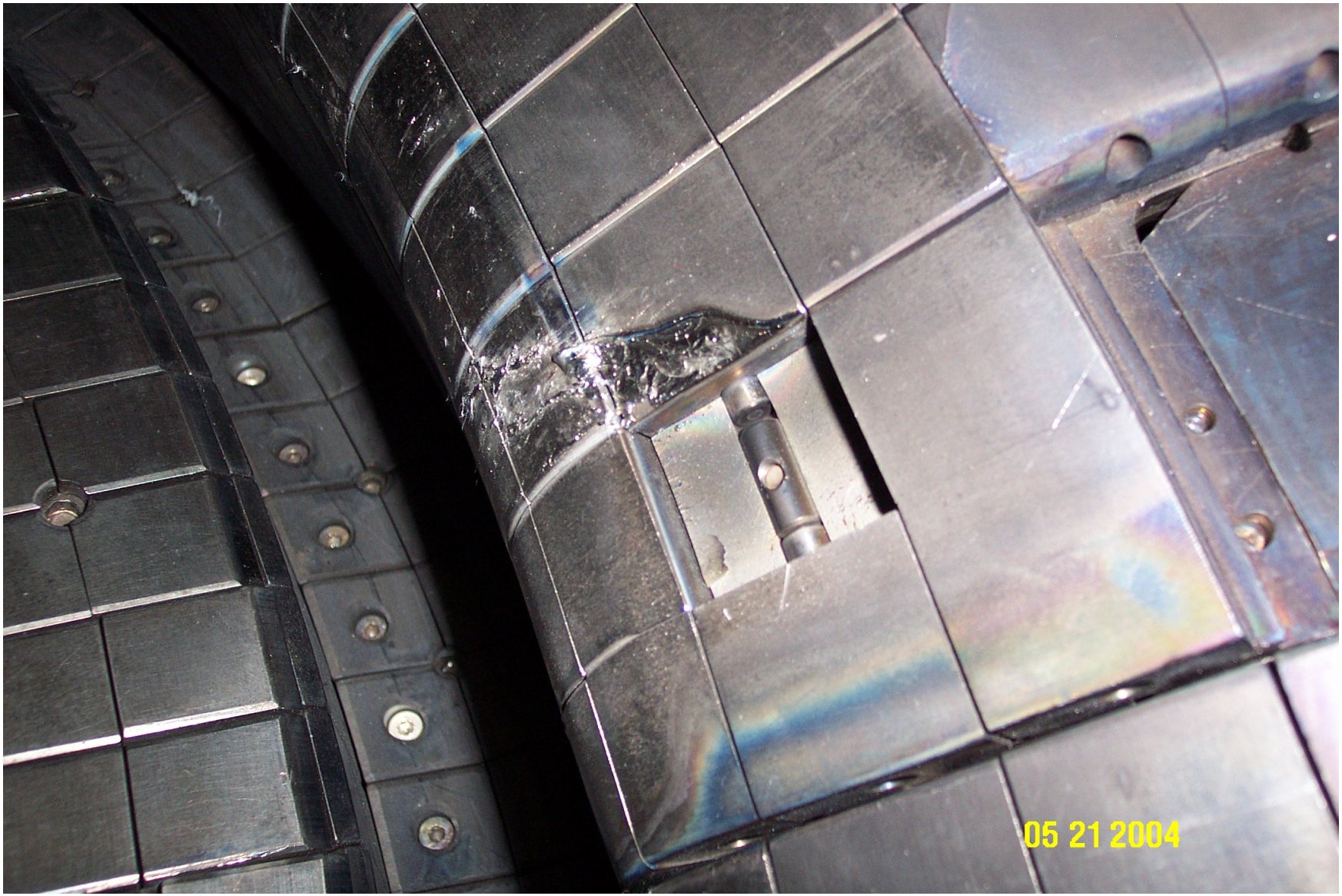

Fig. 1.1 - In-Situ Melting of TZM Molybdenum Mono-Block Tiles

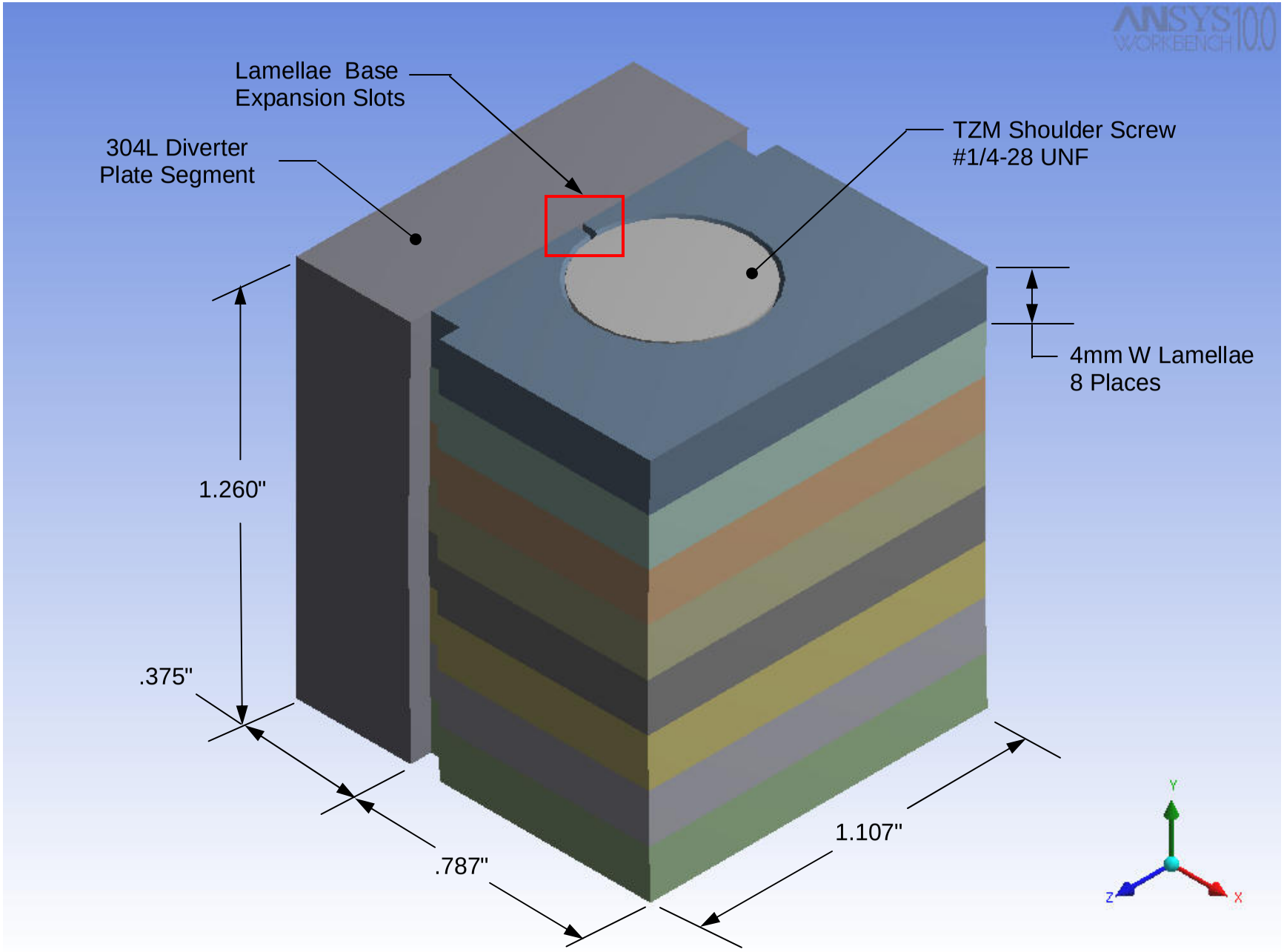

Fig. 2.1.1 - Lamellae W Tile Assembly Full Solid Model

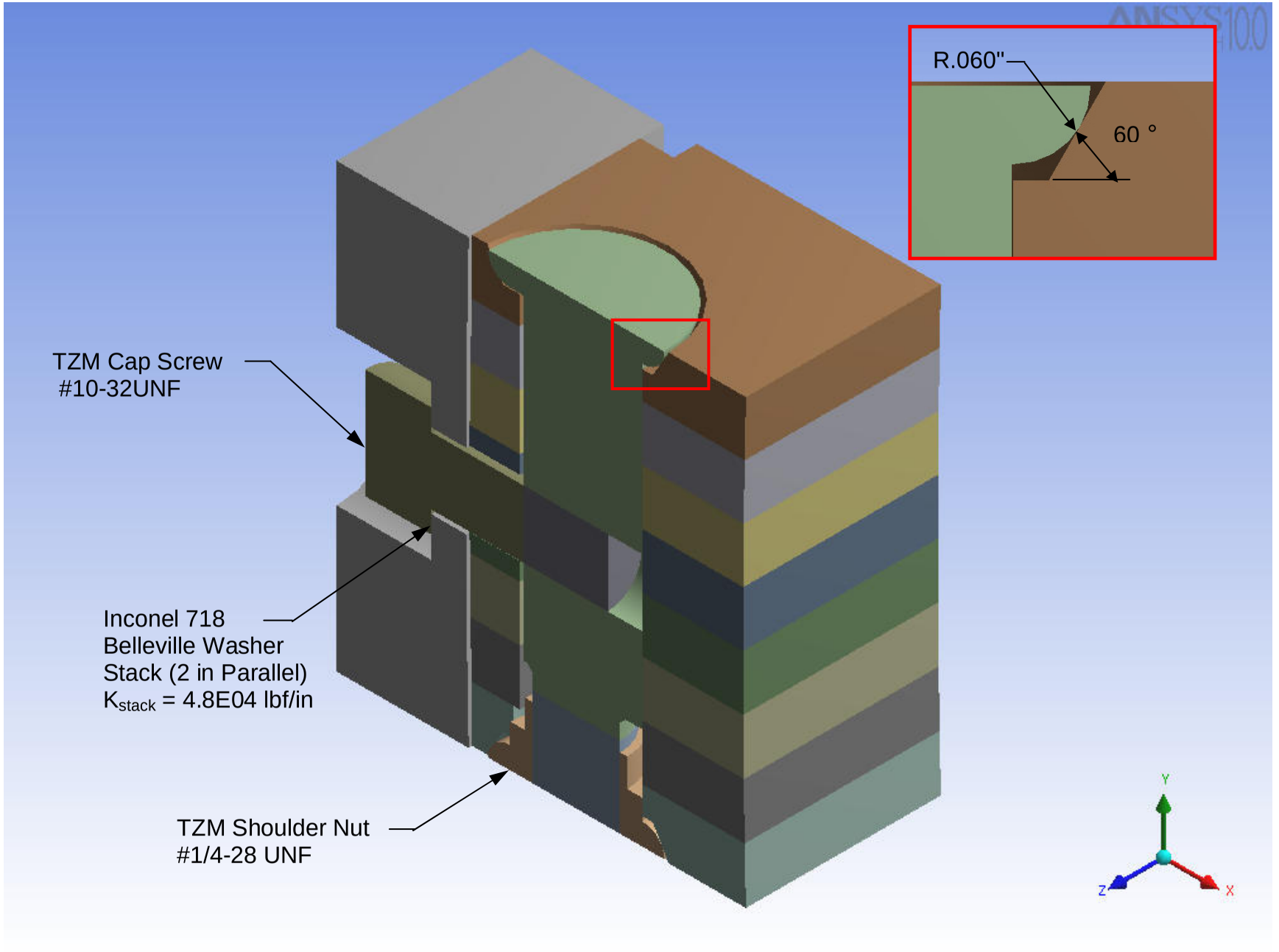

Fig. 2.1.2 - Half Solid Model: Single Plane of Symmetry

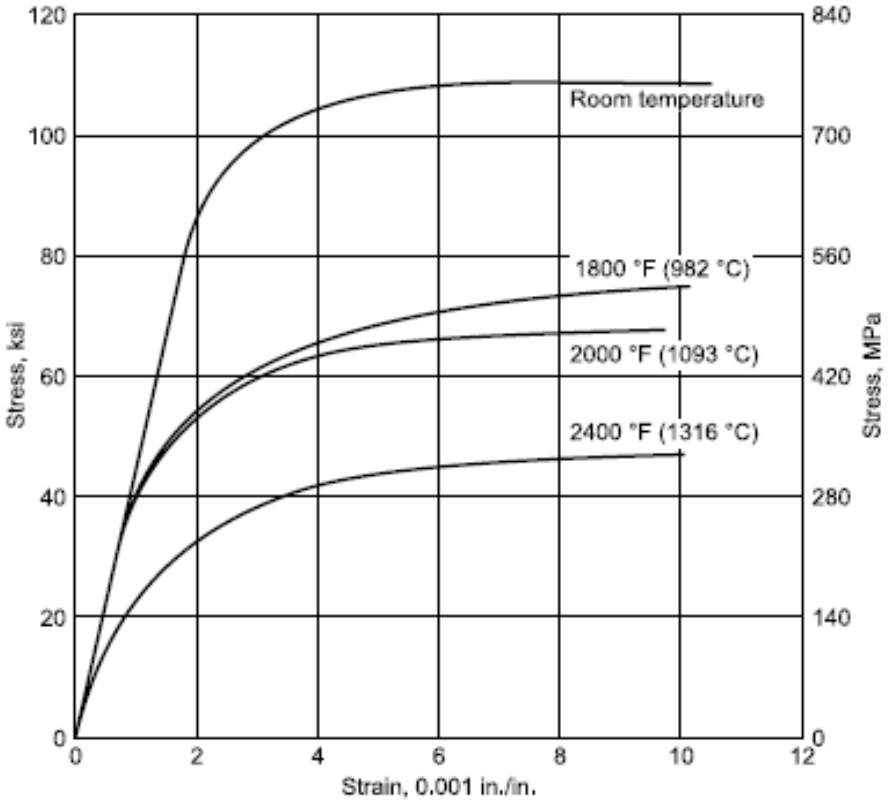

Fig. 2.2.1 -TZM Stress-Strain vs Temperature [4]

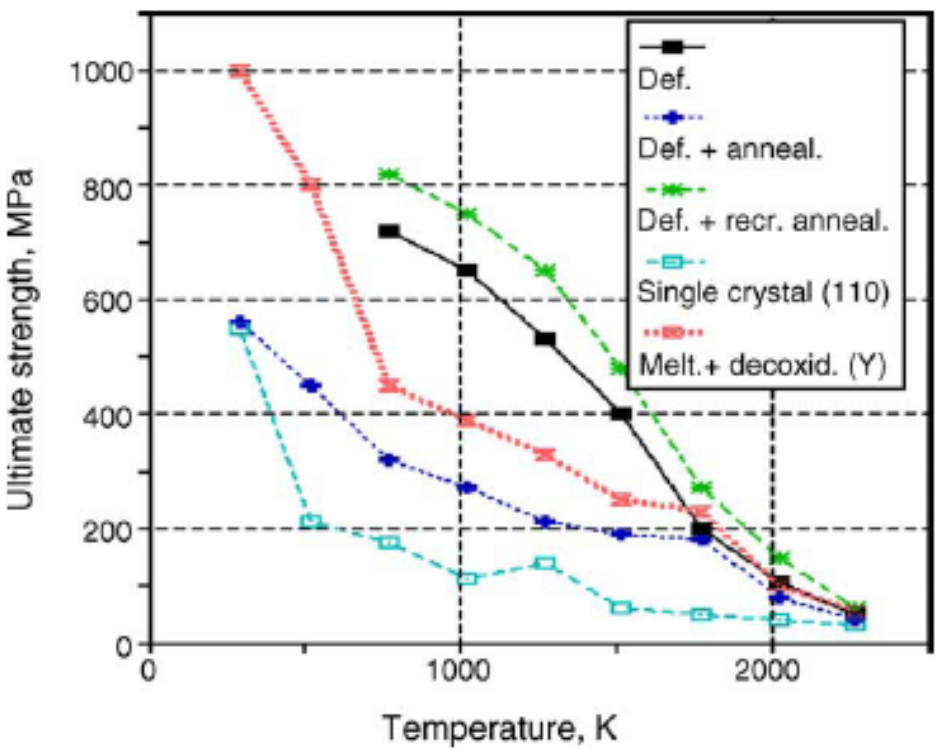

Fig. 2.2.2 - Tungsten Strength vs Temperature [5]

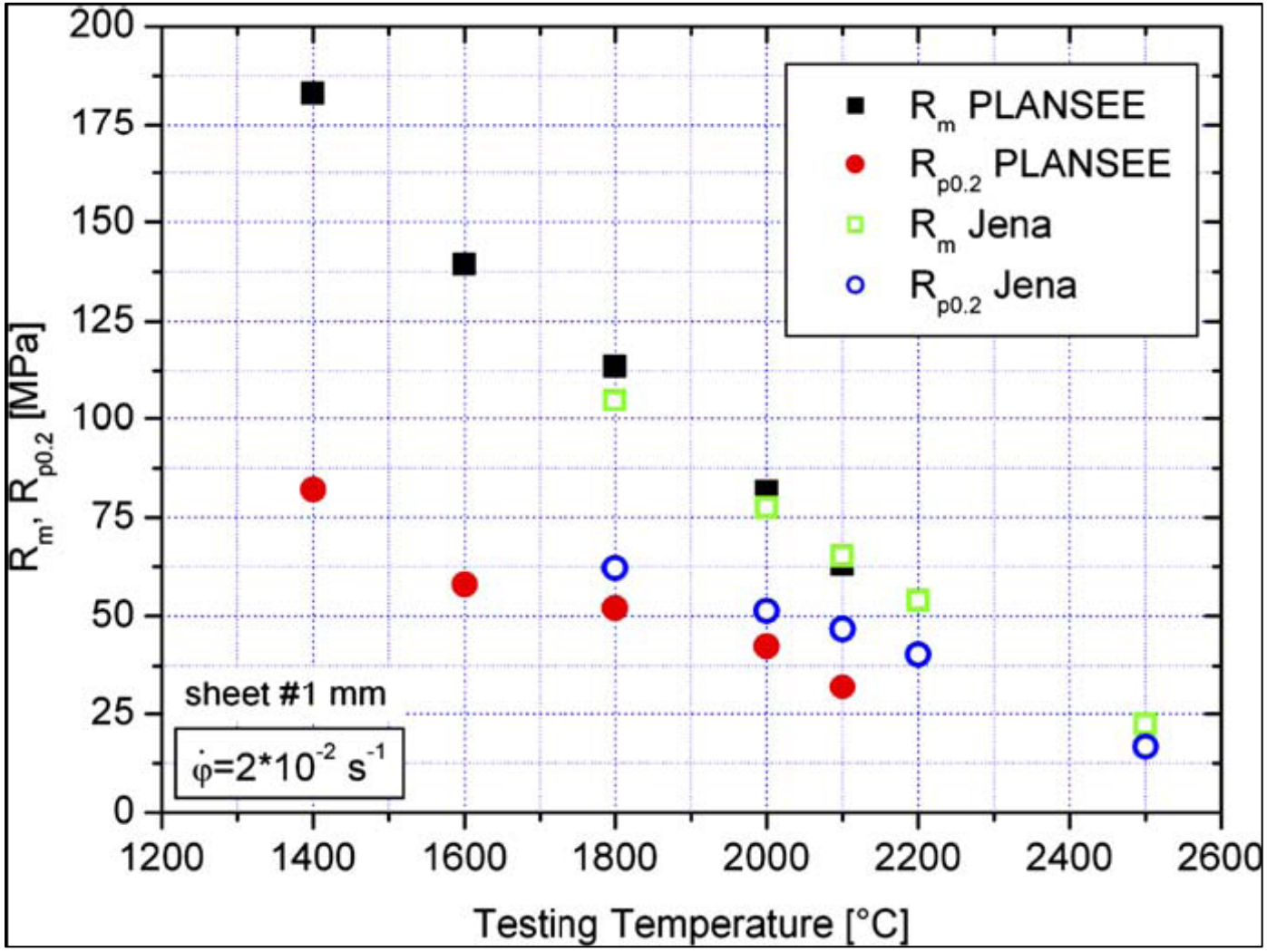

Mean values of mechanical properties of stress-relieved tungsten sheet material (thickness 1mm) between 1400 °C and 2500 °C determined in uniaxial tensile tests with an initial strain rate of $2 * 10^{-2}\ s^{-1}$.

Fig. 2.2.3 - Very High Temperature Strength of PLANSEE W-Sheet [6]

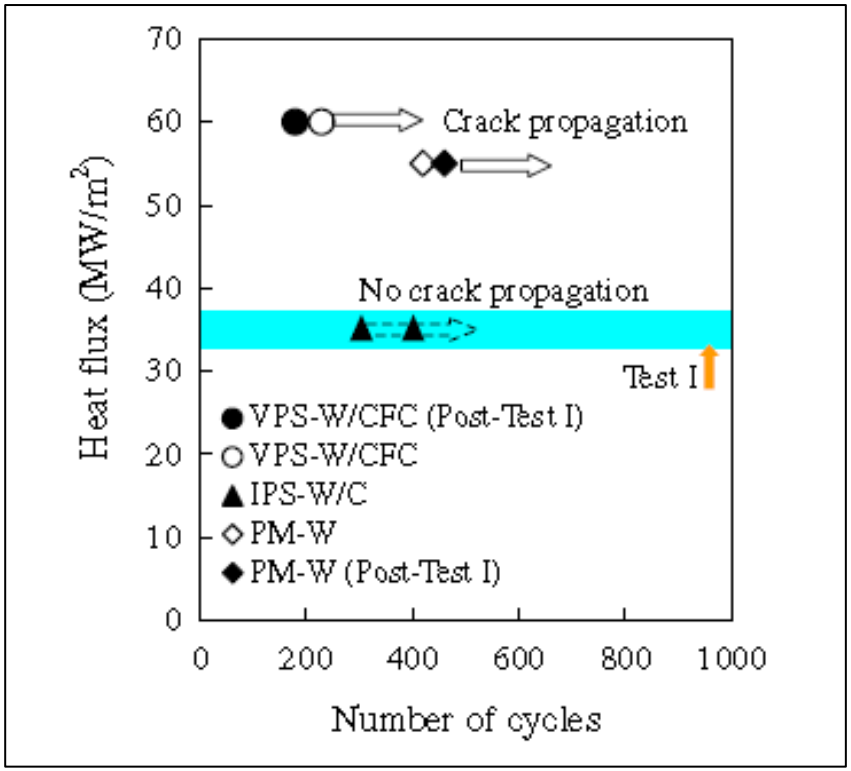

A relationship of crack formation with heat flux and the number of cycles.

Cycles [7] Fig. 2.2.4 - W-Sheet Crack Formation vs Heat Flux and Number of

Sample Size =10 mm x 10 mm x 2.5 mm, Surface Temp = 2000-2200 C

Fig. 2.2.5 - Composite Tungsten and TZM Molybdenum Strength vs Temperature Curves Used to Evaluate Results

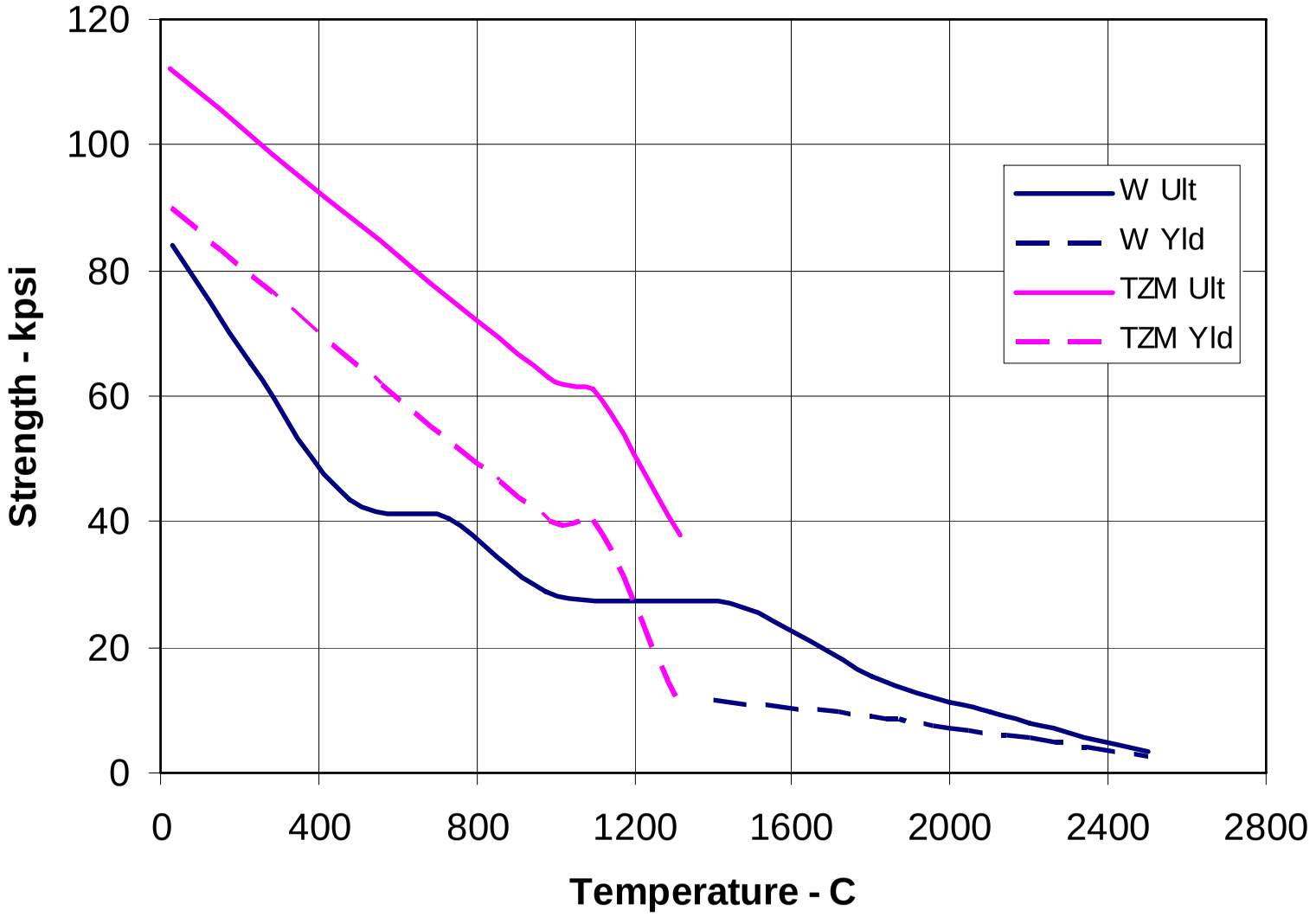

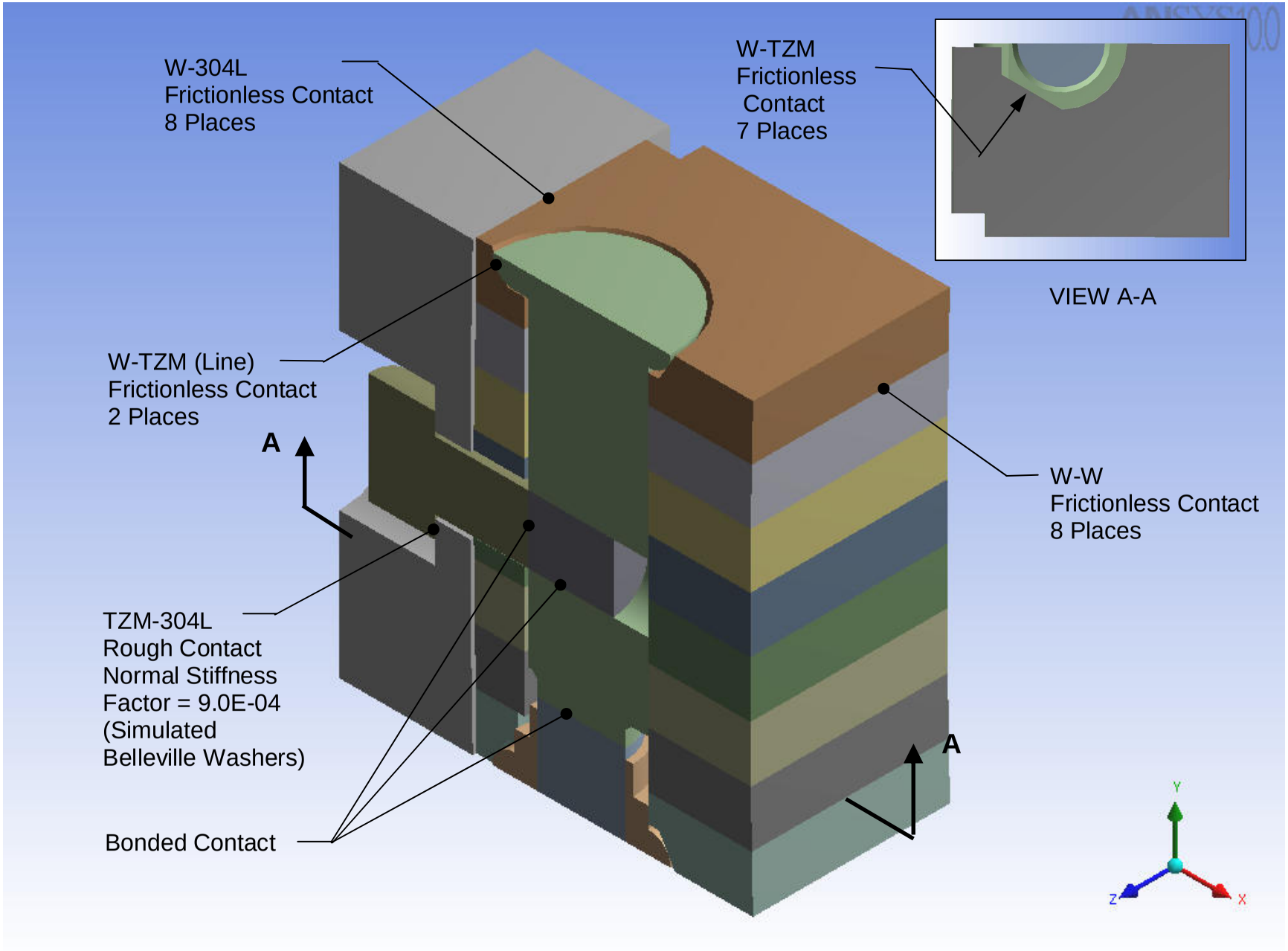

Fig. 2.3.1 - Mechanical and Thermal Contact

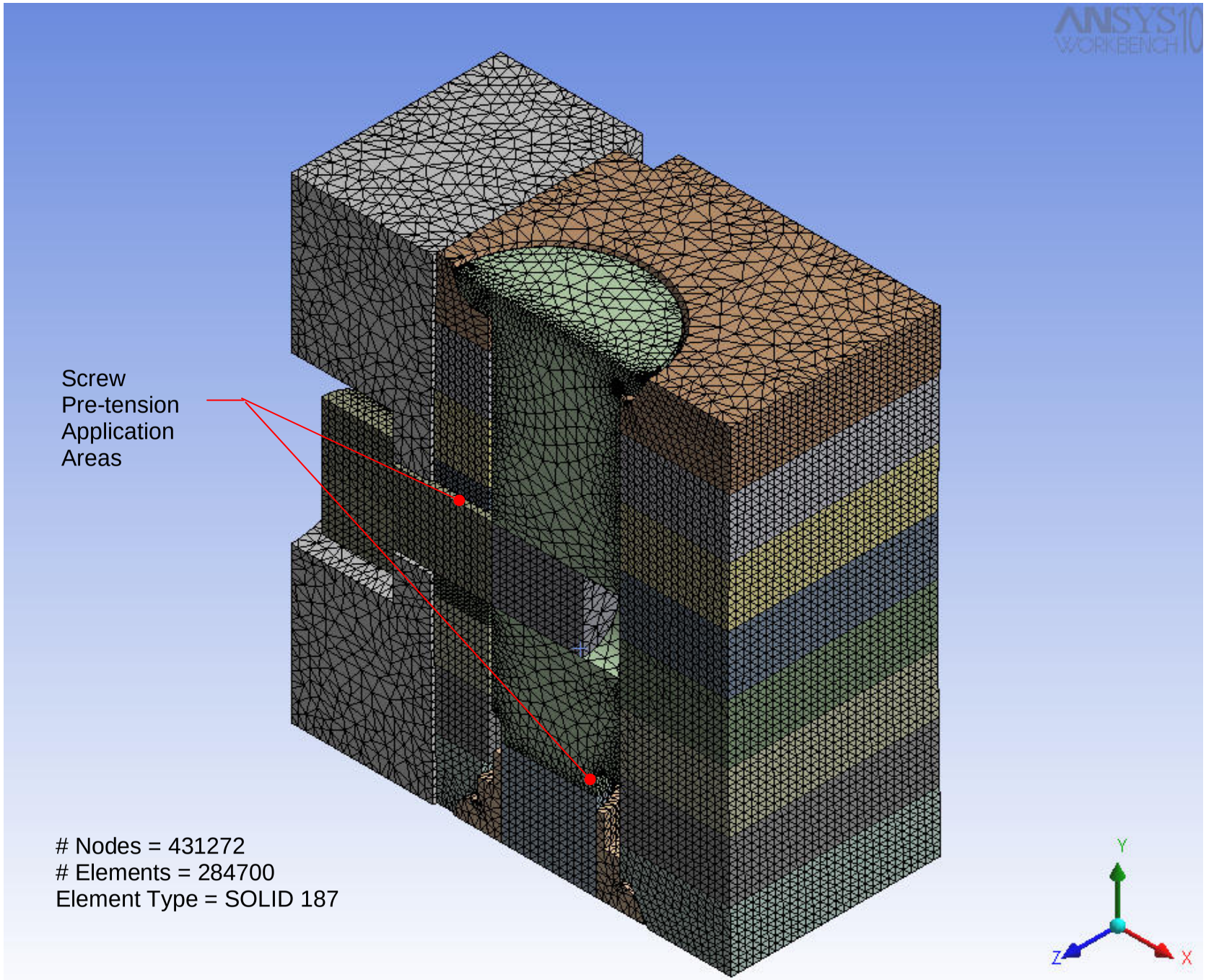

Fig. 2.4.1 - ANSYS Automatically Generated Mesh

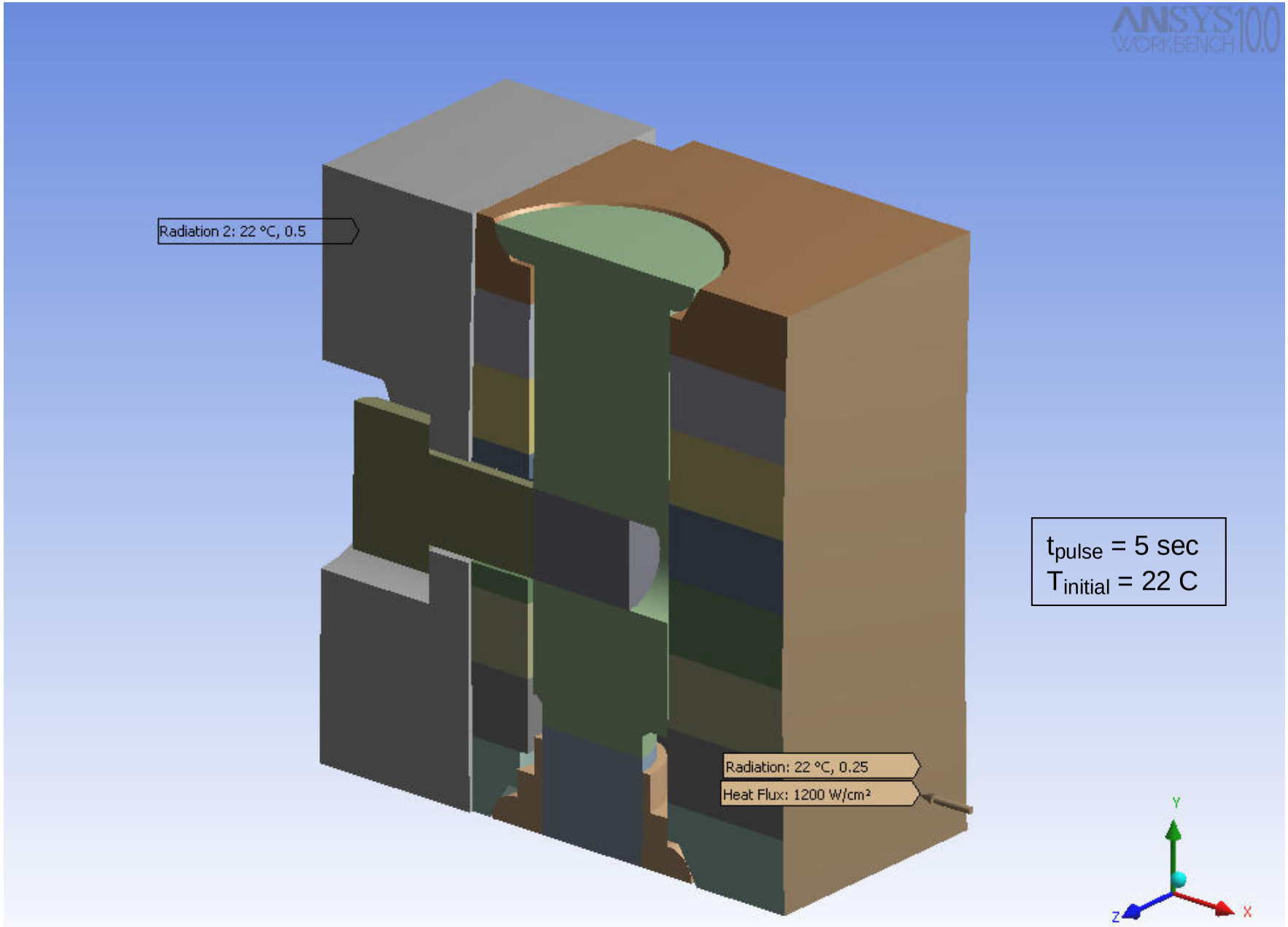

Fig. 2.5.1 - Nonlinear Transient Thermal Model Boundary Conditions

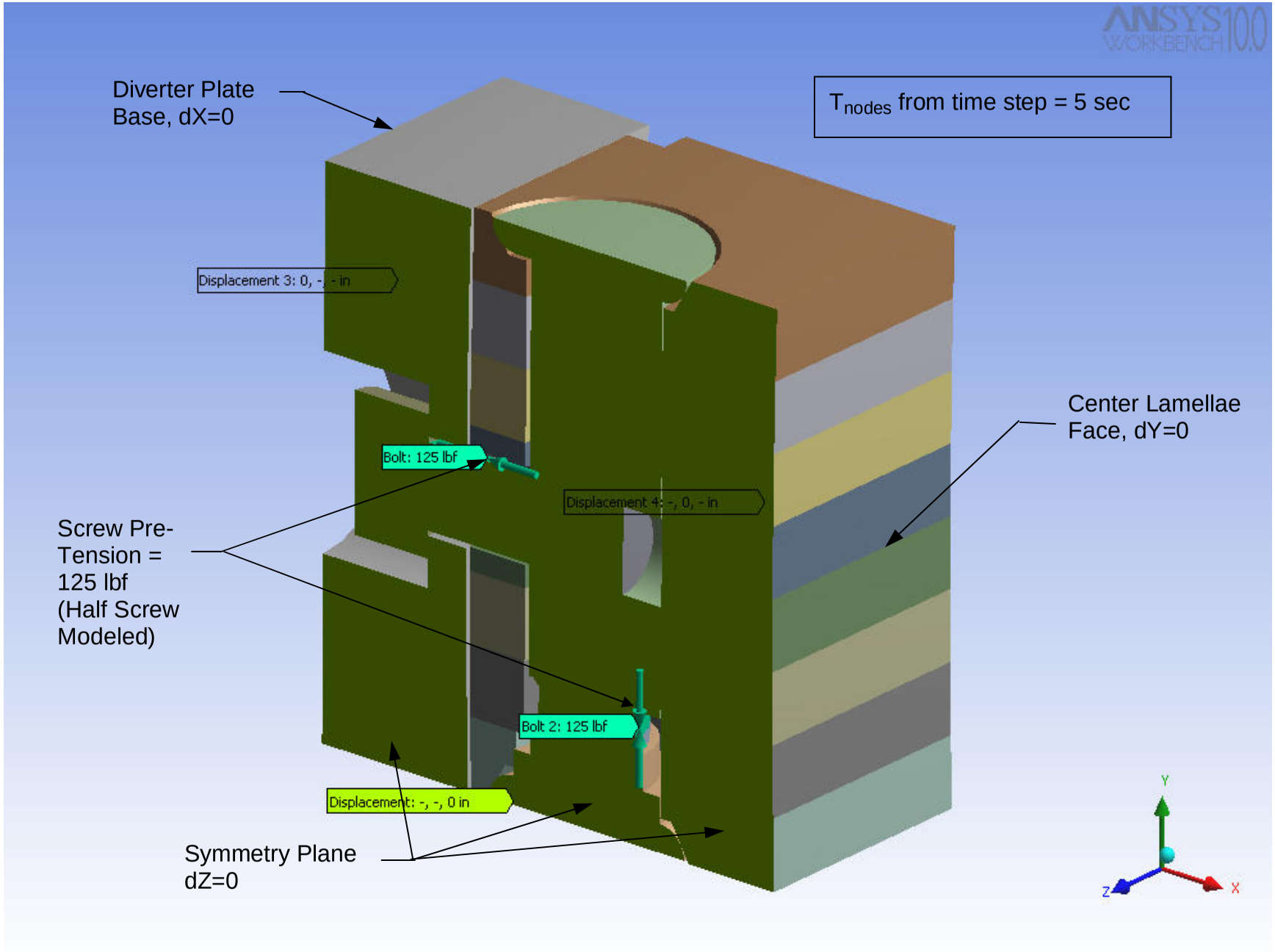

Fig. 2.5.2 - Nonlinear Thermal Stress Model Boundary Conditions

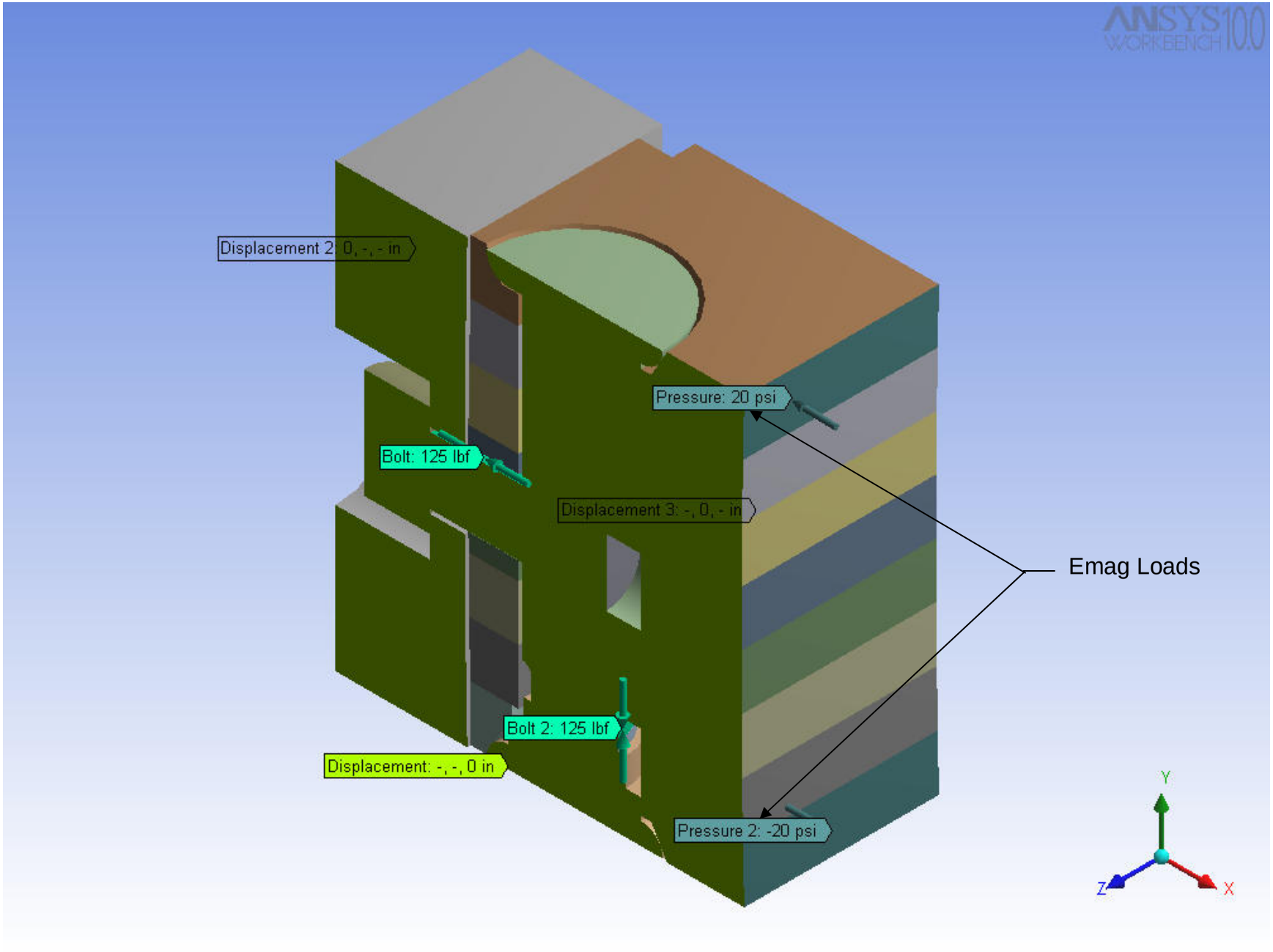

Fig. 2.5.3 - Nonlinear Thermal Stress + Emag Load Model B.C.'s

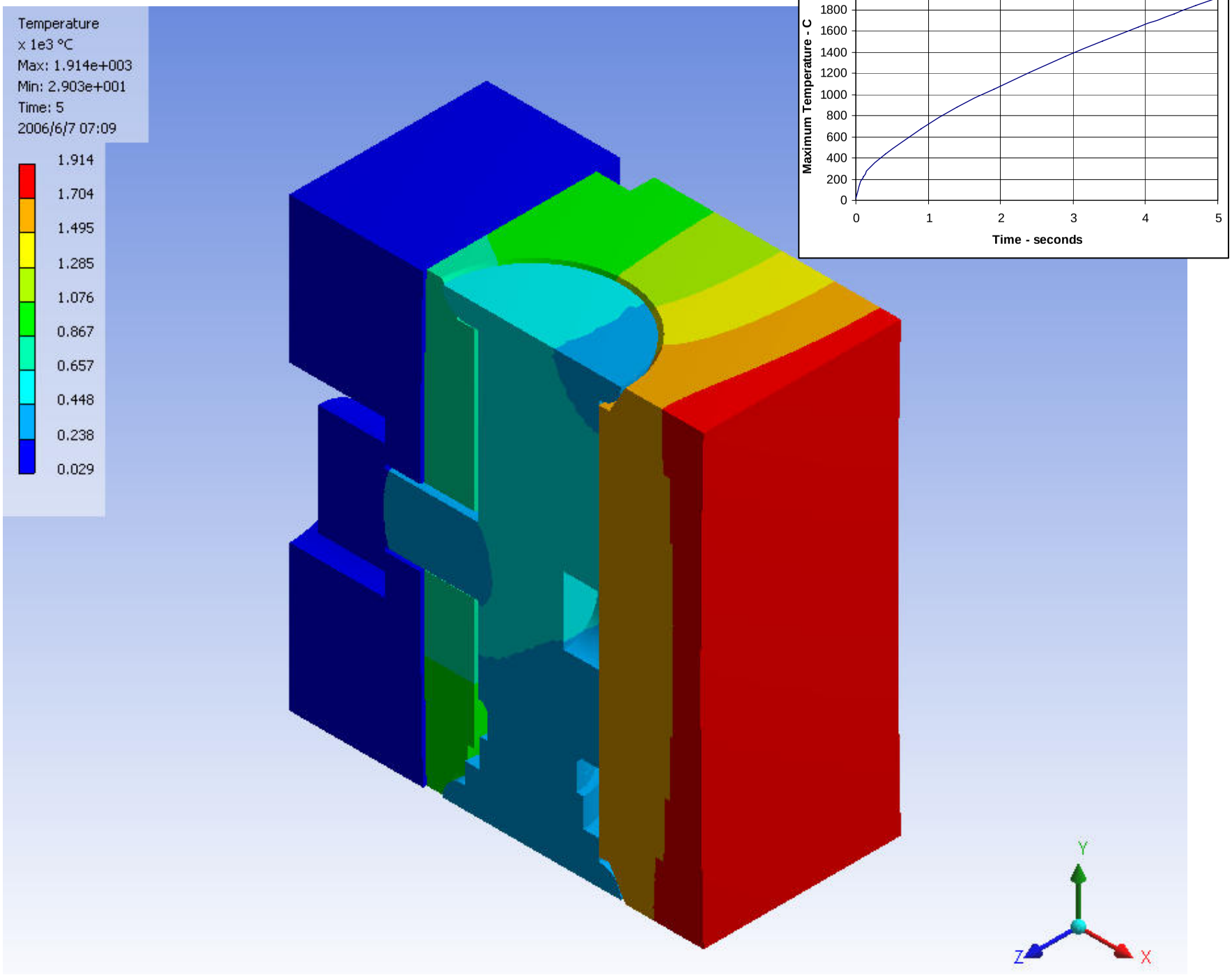

Fig. 3.1.1 - Thermal Model: Temperature Profile at Time Step = 5 Sec.

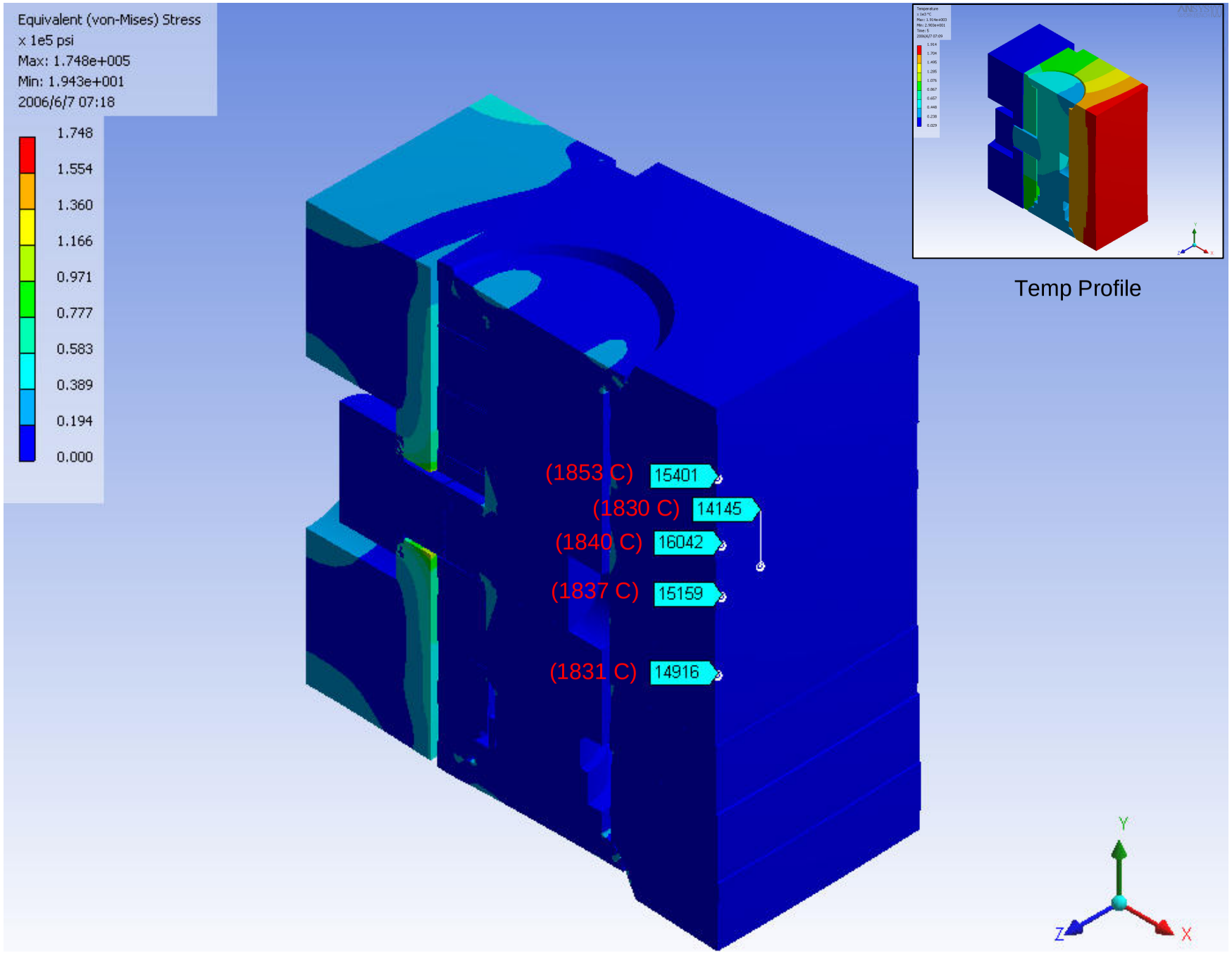

Fig. 3.2.1 - Thermal Stress Model: von Mises; IsoView

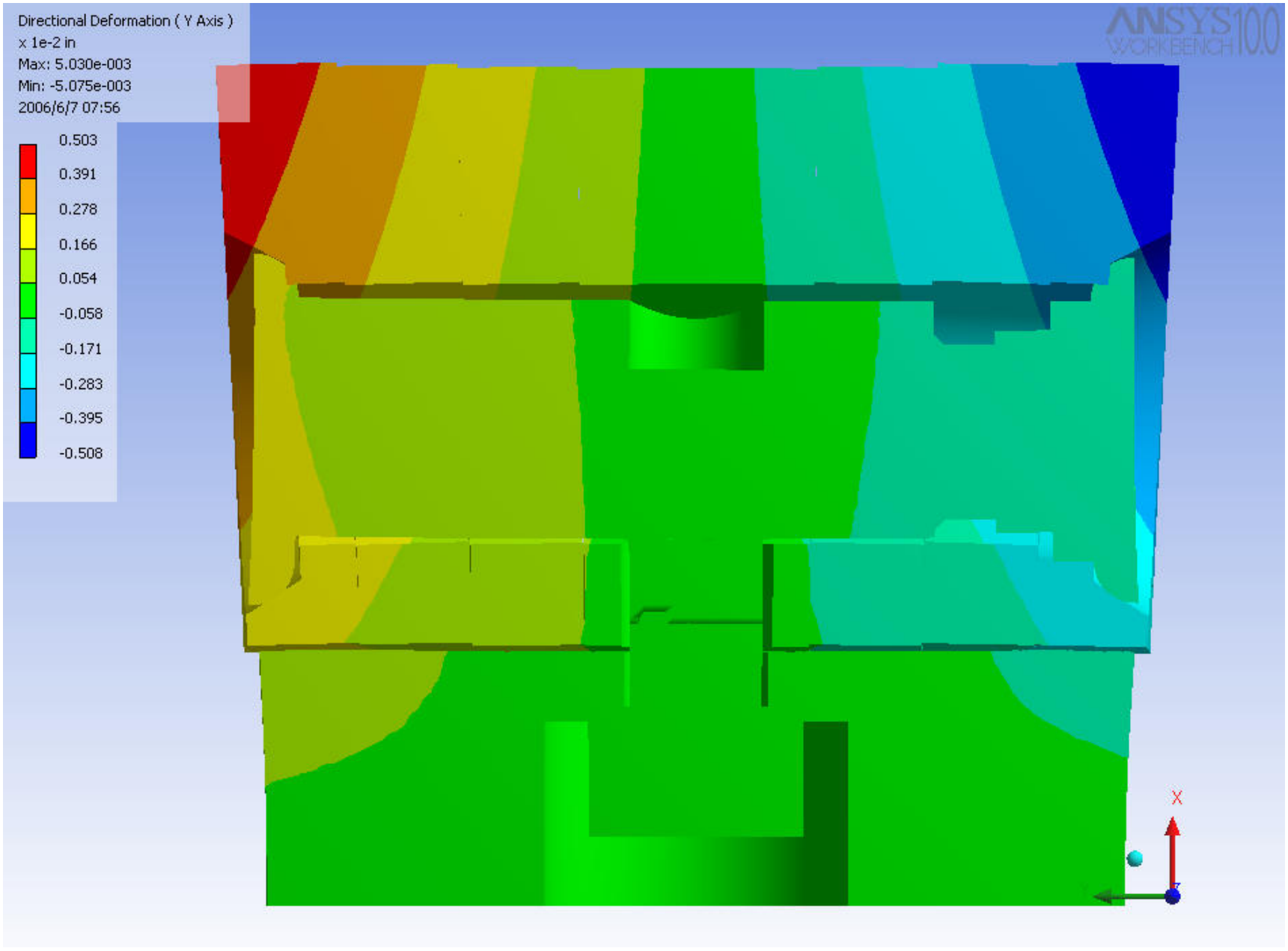

Fig. 3.2.2 - Thermal Stress Model: Y Axis (Circumferential) Deformation

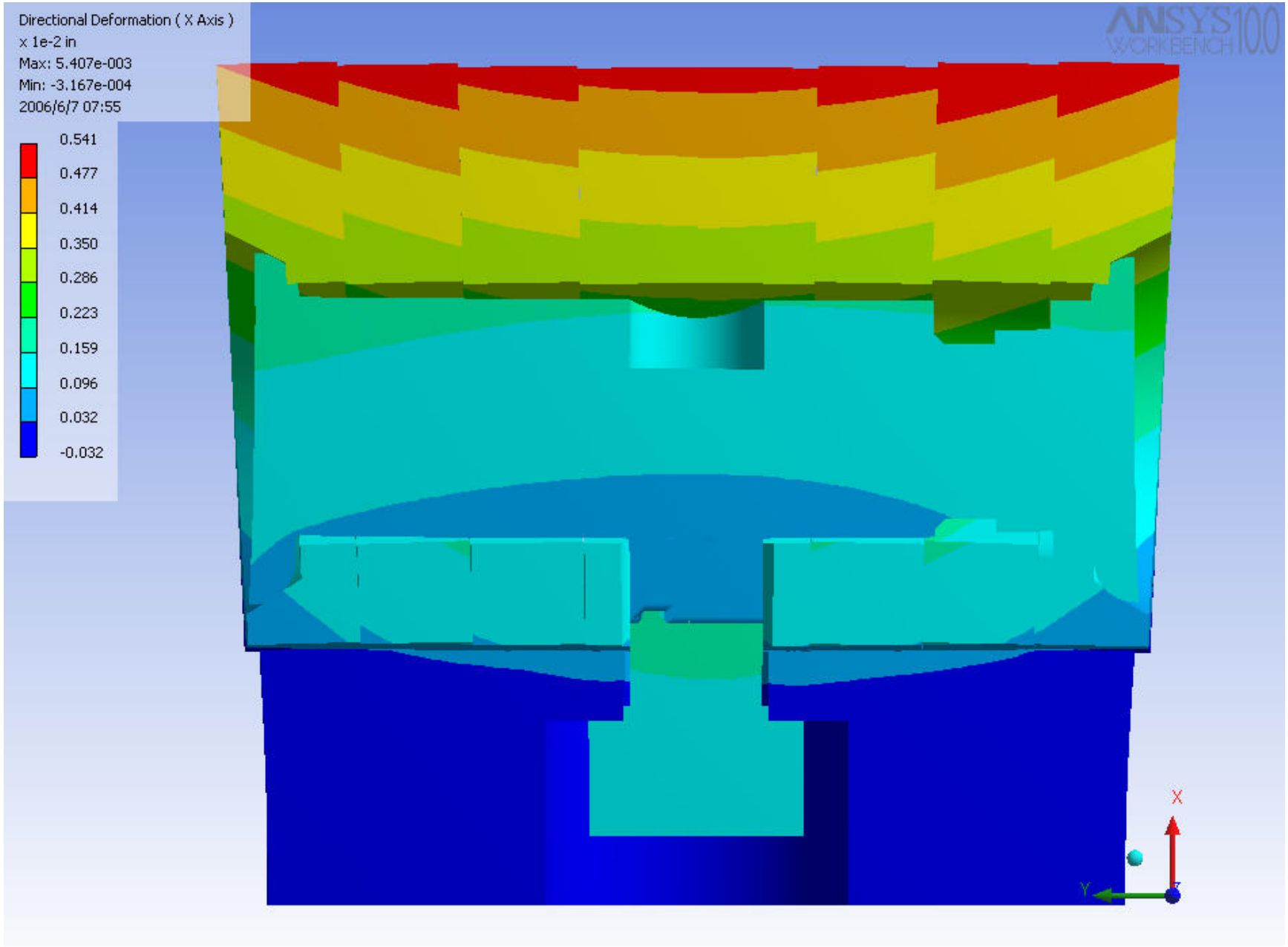

Fig. 3.2.3 - Thermal Stress Model: X Axis (Radial) Deformation

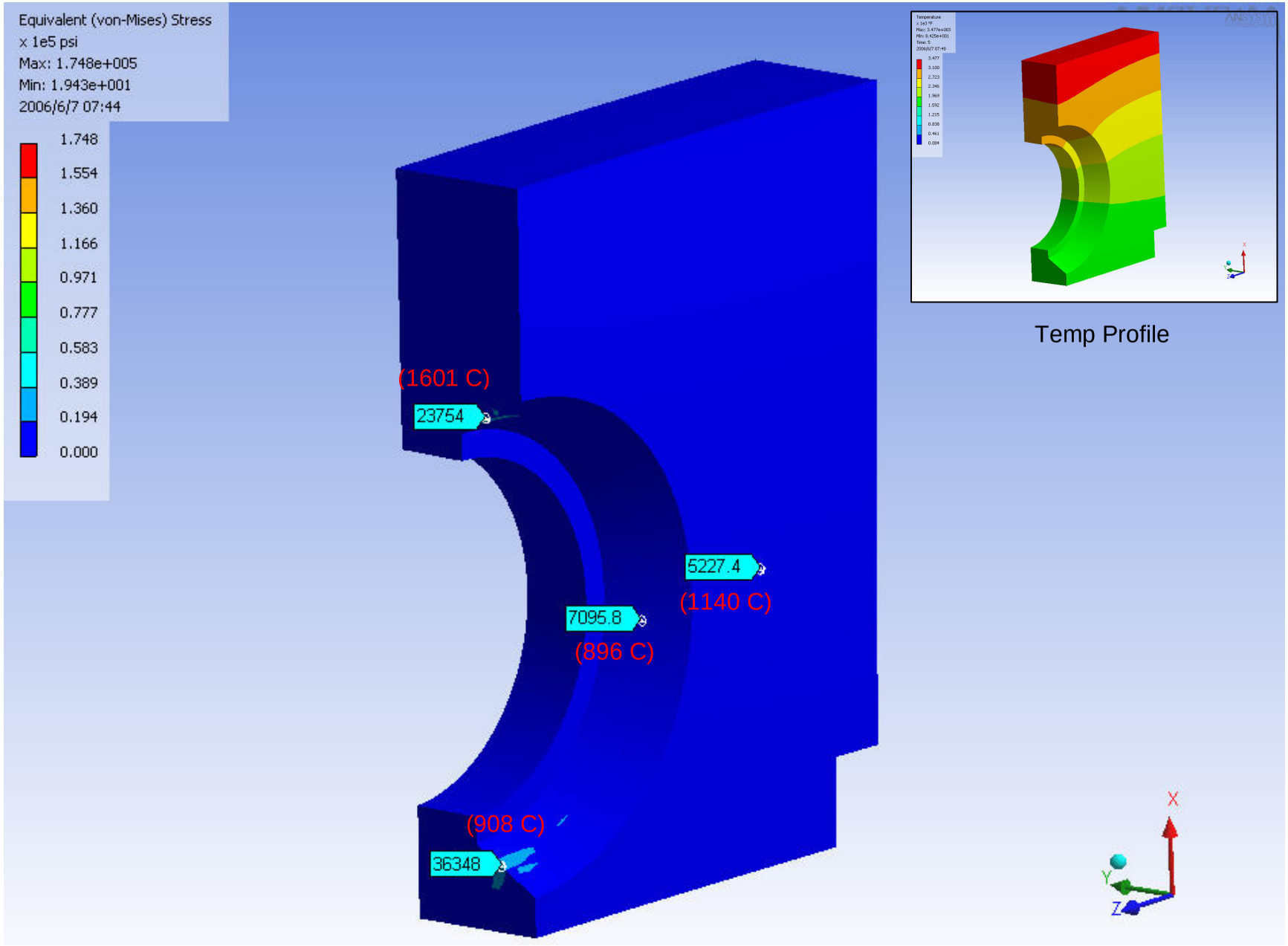

Fig. 3.2.4 - Thermal Stress Profile: von Mises; Nut Endplate View

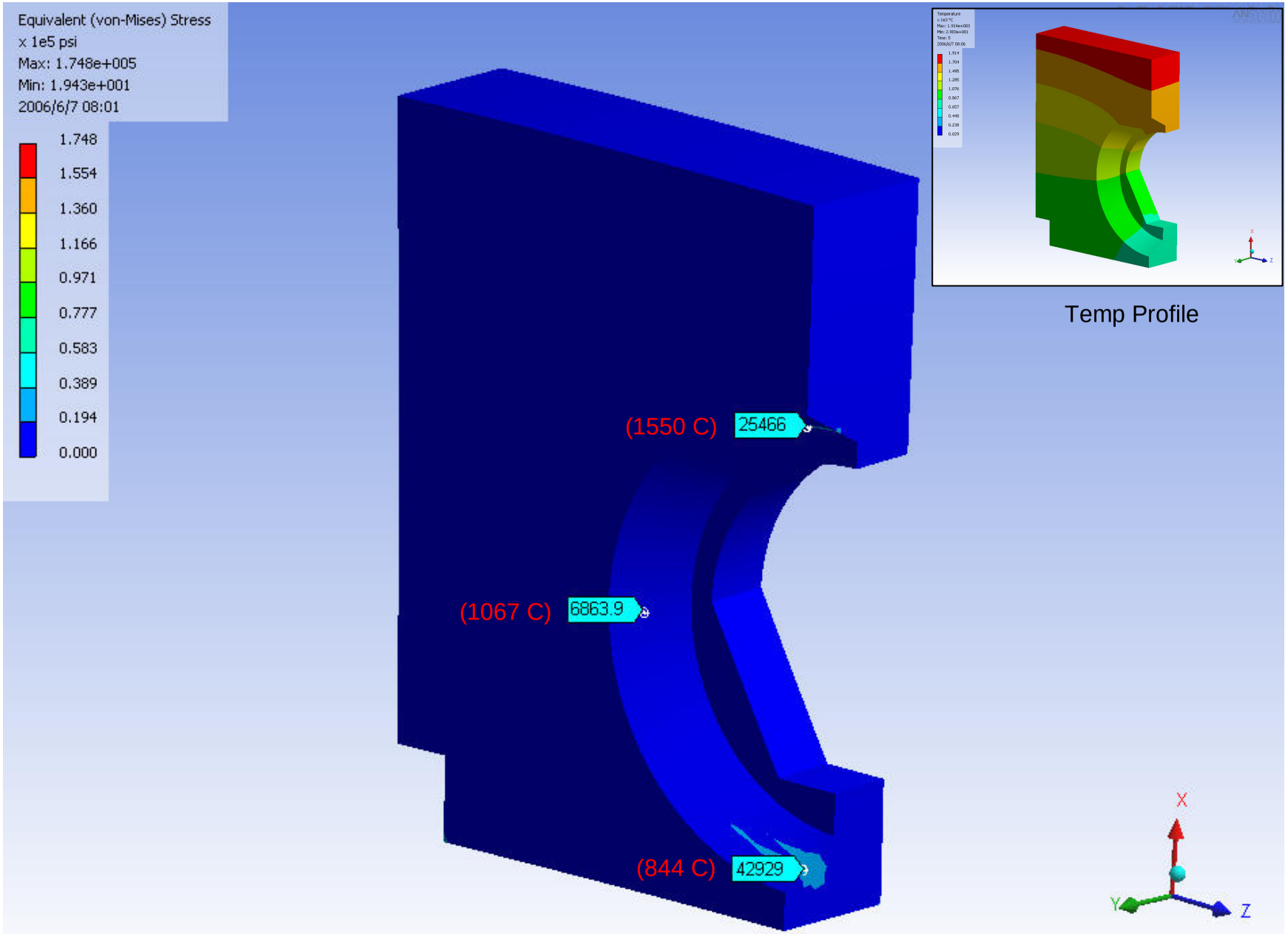

Fig. 3.2.5 - Thermal Stress Profile: von Mises; Screw Head Endplate View

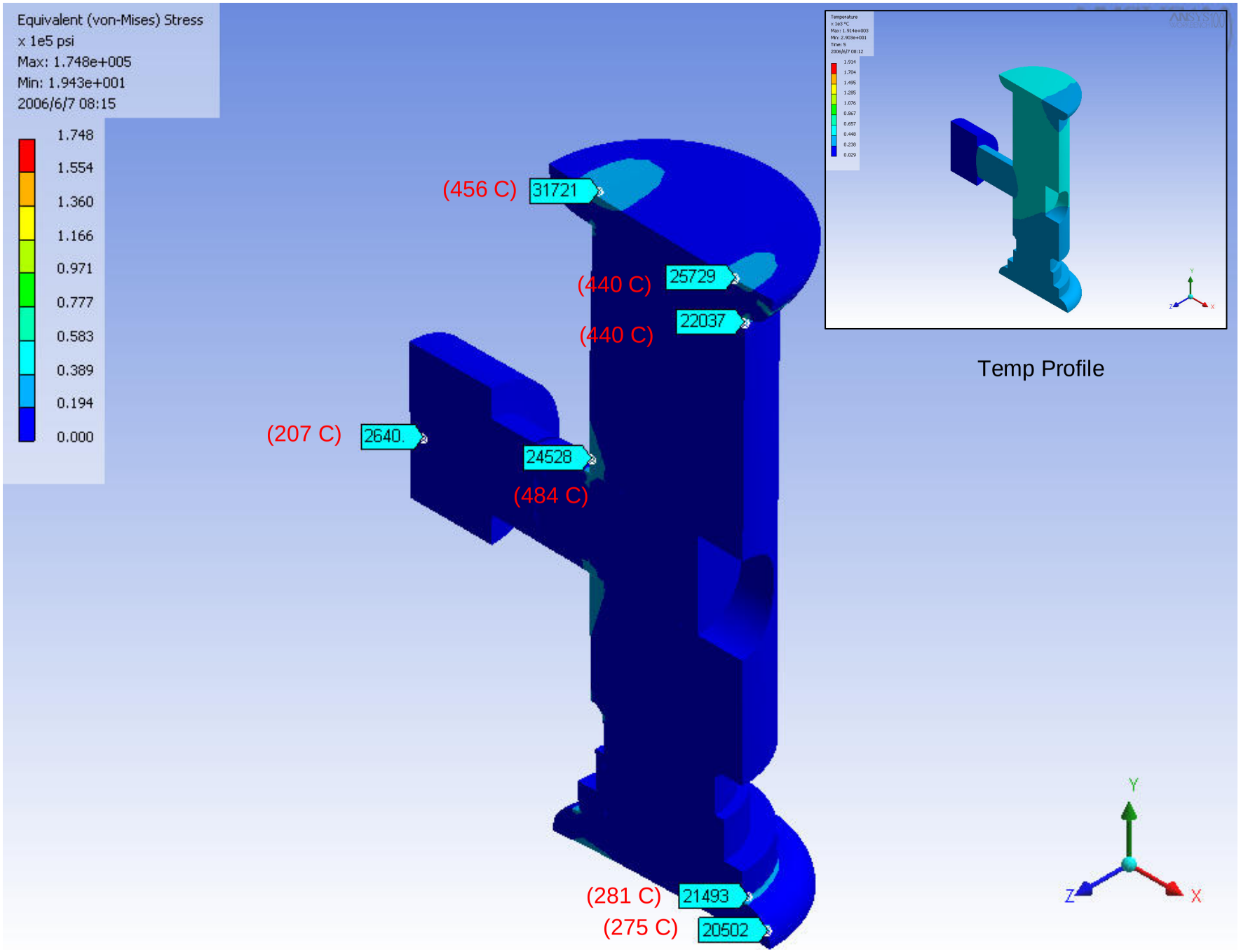

Fig. 3.2.6 - Thermal Stress Profile: von Mises; Screw Assy View 1

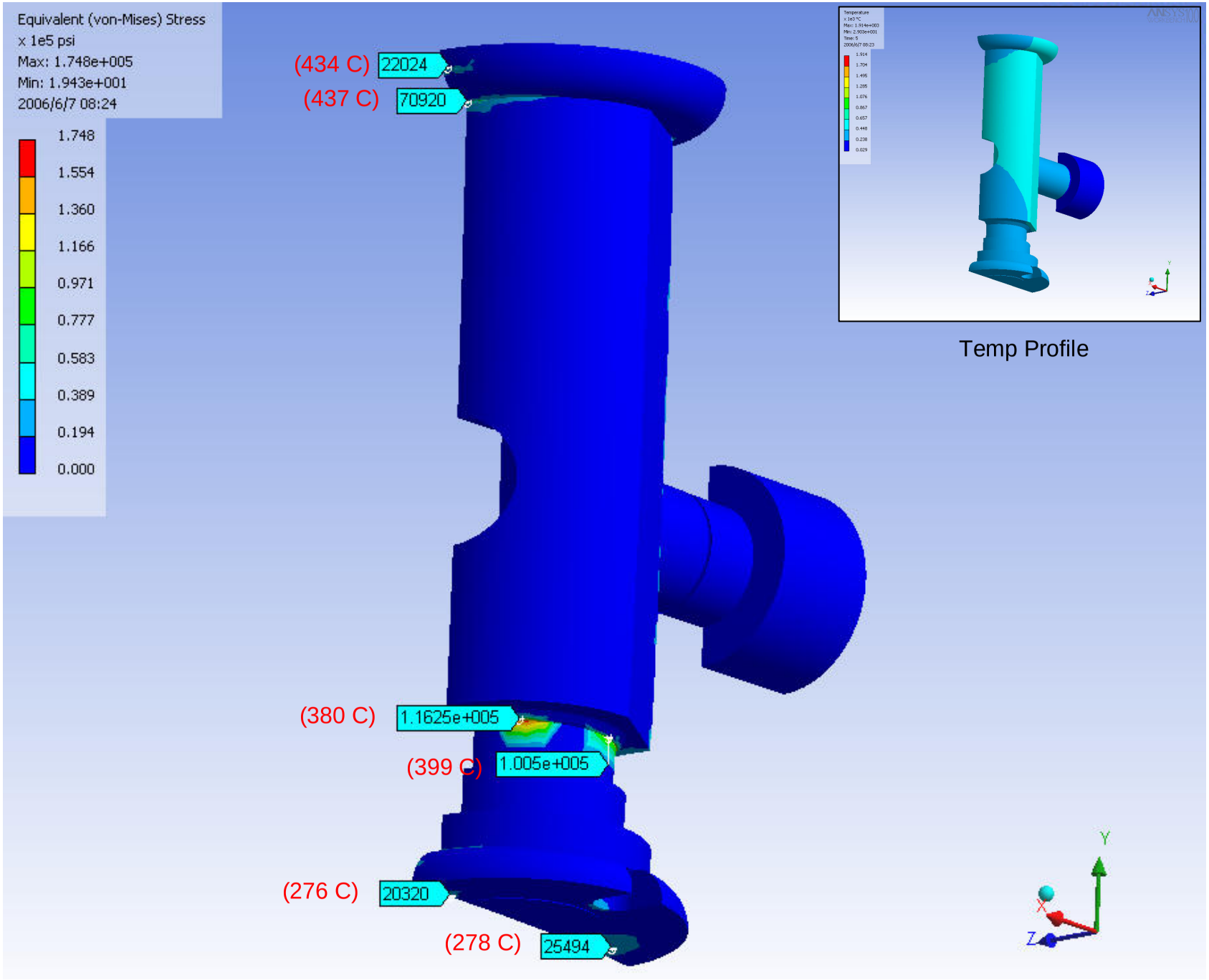

Fig. 3.2.7 - Thermal Stress Profile: von Mises, Screw Assy View 2

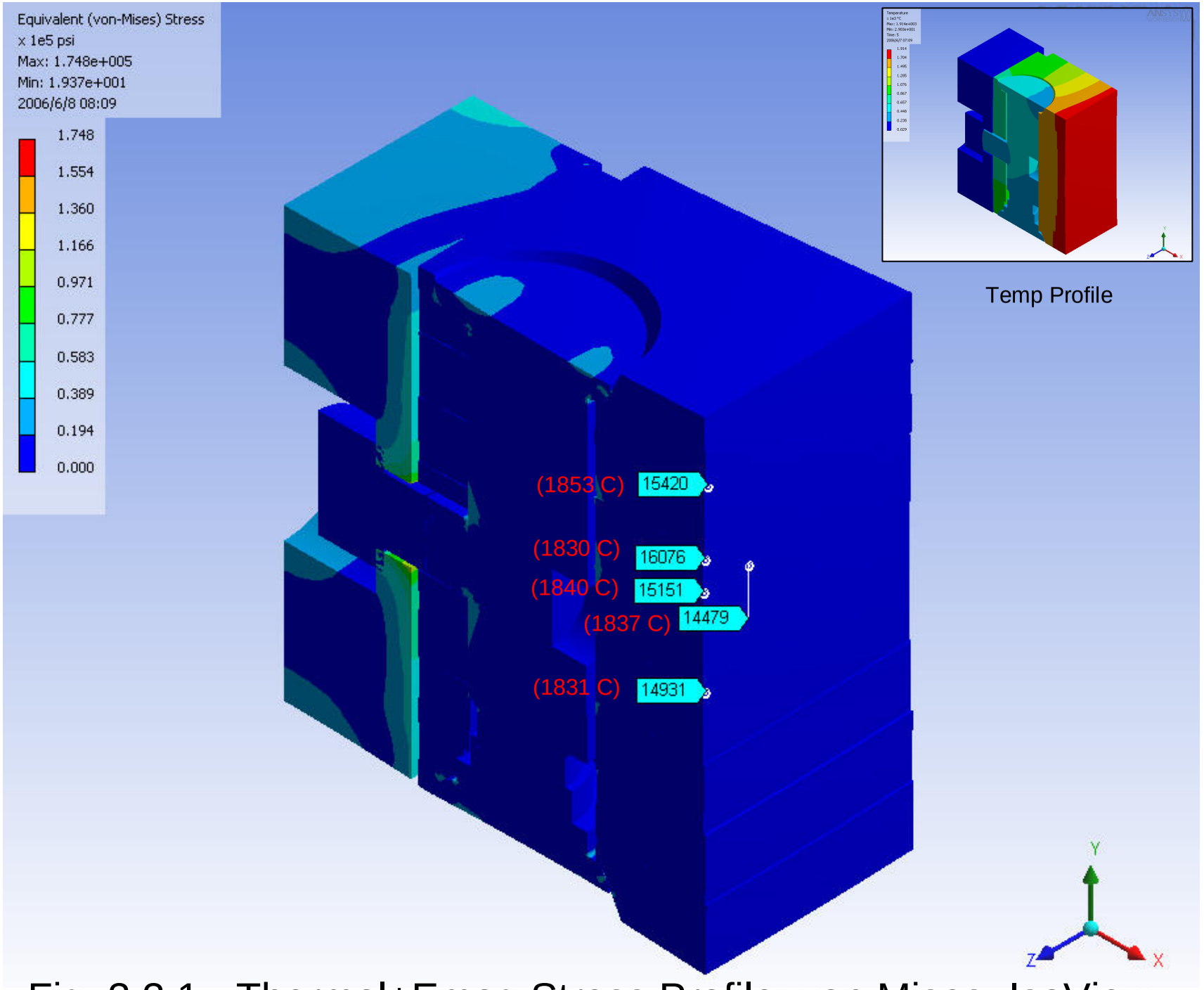

Fig. 3.3.1 - Thermal+Emag Stress Profile: von Mises, IsoView

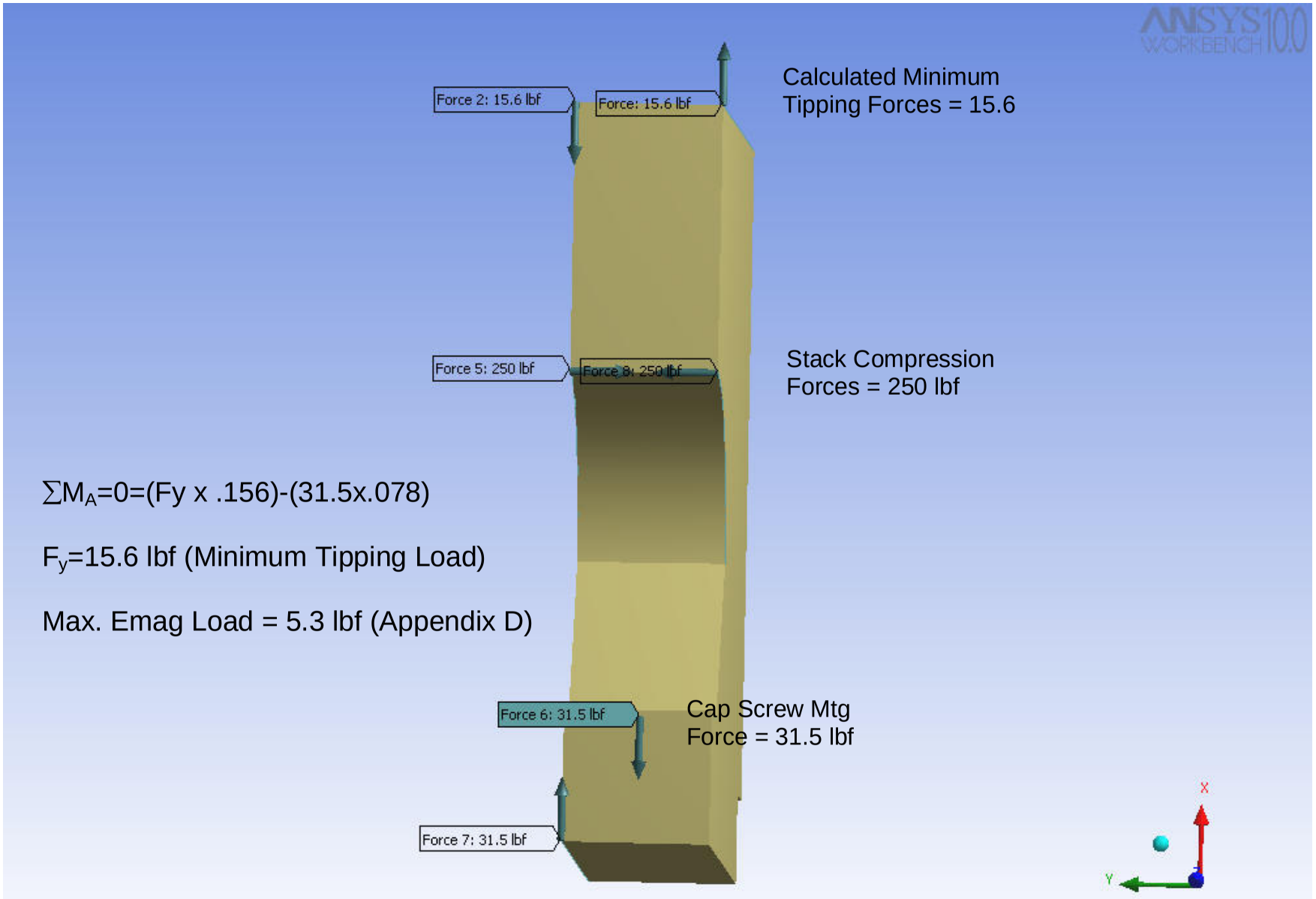

Fig. 3.4.1 - Single Lamella Free Body Diagram:
Minimum Emag Tipping Load

Appendix A
Lamellae Tile Design Fabrication Drawings

REVISIONS				
ZONE	REV.	DESCRIPTION	DATE	APPROVED
	A	ORIGINAL ISSUE	- - -	- - -

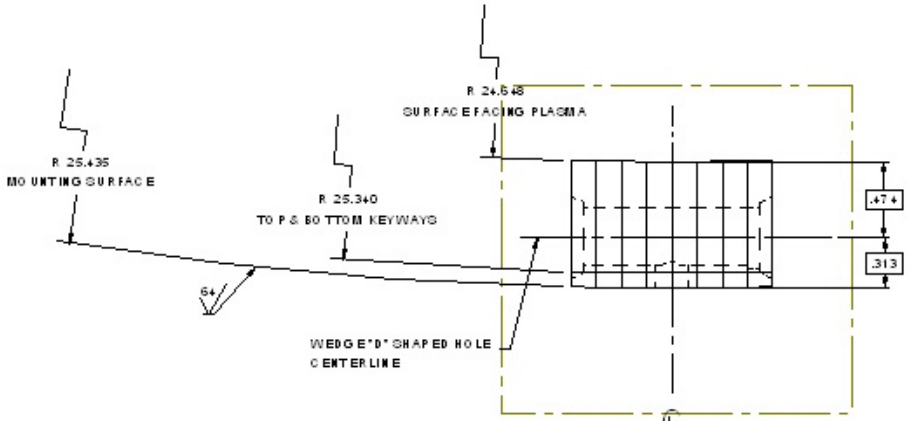

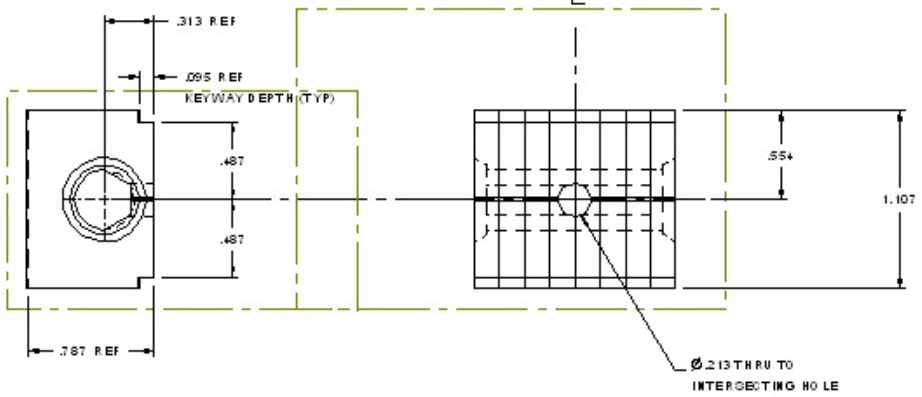

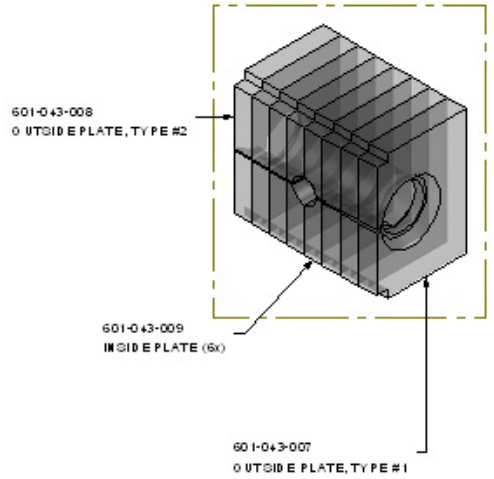

USED ON ASSEMBLY	PLASMA SCIENCE & FUSION CENTER	ITEM	PART NO.	DESCRIPTION	QTY.
601-043-000	MASSACHUSETTS INSTITUTE OF TECHNOLOGY			FINAL MACHINING, WEDGE "D" TYPE ASSY. TUNGSTEN PLATE TILE #75 - NO TAPERS	DWG C SIZE
	TOLERANCES UNLESS OTHERWISE SPECIFIED: DECIMALS 3 PLACES ±.005, 2 PLACES ±.010, 1 PLACE ±0.10; ANGLES ±0° 15'; 125 ✓ REMOVE ALL BURRS; BREAK SHARP EDGES; DO NOT SCALE DRAWING	DRAWN	GAVELLI	DATE 6 MAR 06	DWG NO. 601-043-000	REV A
		CHECKED		DATE		
		APPROVED		DATE		
		CAD FILE:		SCALE 2:1	SHEET: 1 OF 1	

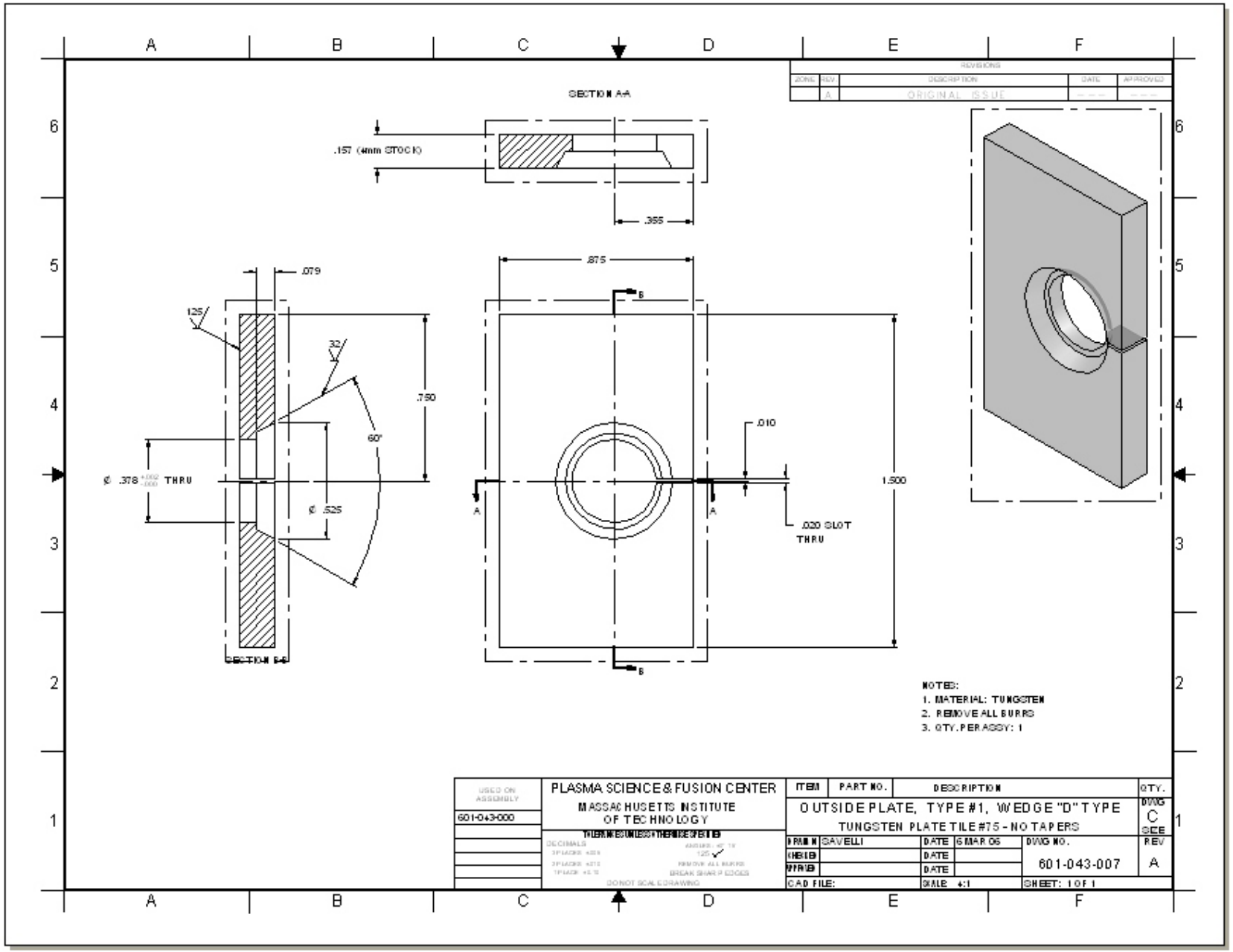
SECTION A-A
.157 (4mm STOCK)
.355
.875
.079
125
32
.750
60°
Ø .378 +.002 -.000 THRU
Ø .525
SECTION B-B
B
.010
.020 SLOT THRU
1.500
A
NOTES:
1. MATERIAL: TUNGSTEN
2. REMOVE ALL BURRS
3. QTY. PER ASSY: 1
PLASMA SCIENCE & FUSION CENTER
MASSACHUSETTS INSTITUTE OF TECHNOLOGY
OUTSIDE PLATE, TYPE #1, WEDGE "D" TYPE
TUNGSTEN PLATE TILE #75 - NO TAPERS
SAVELLI
6 MAR 06
601-043-007
A
SCALE 4:1
SHEET: 1 OF 1

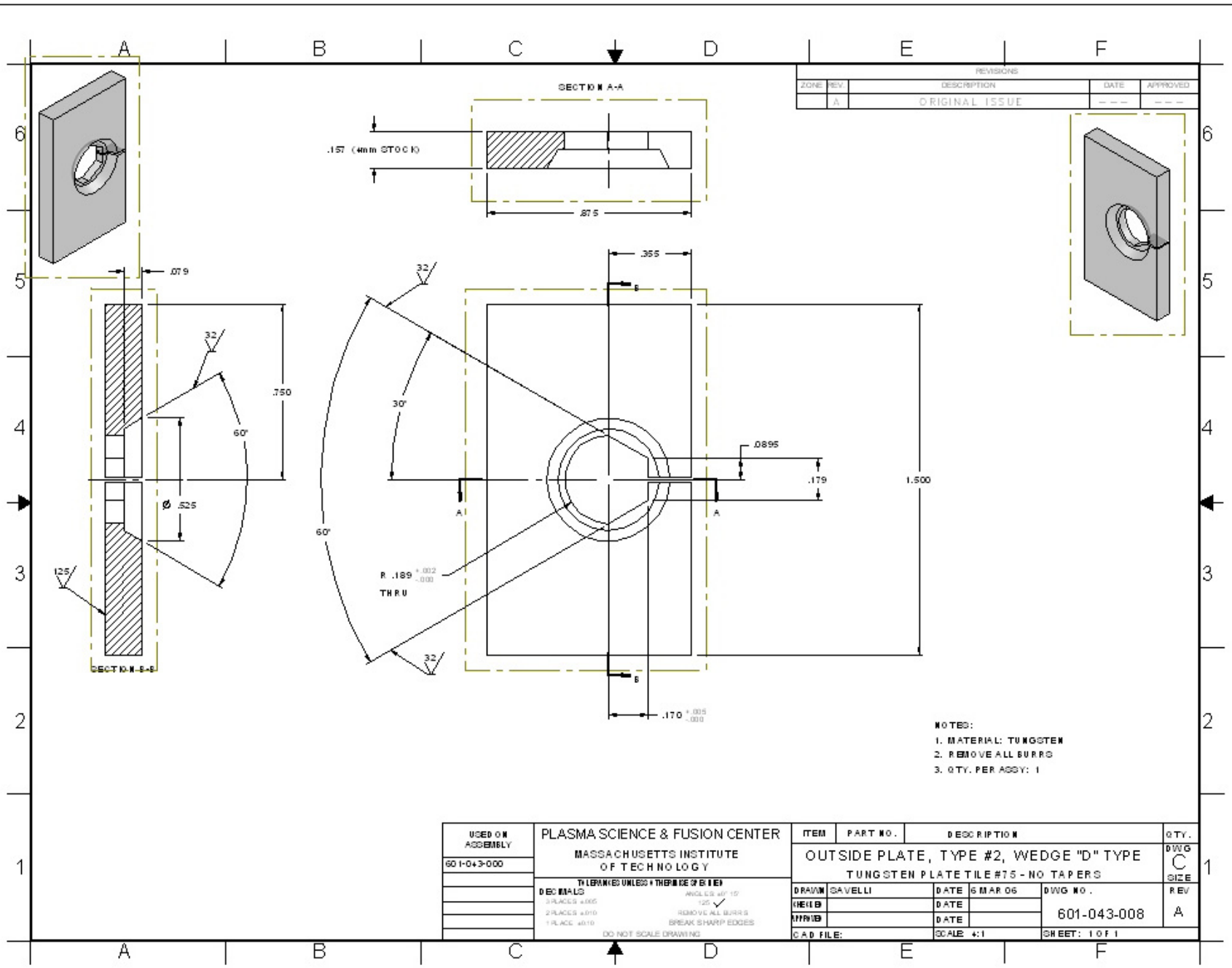

REVISIONS				
ZONE	REV.	DESCRIPTION	DATE	APPROVED
	A	ORIGINAL ISSUE	- - -	- - -

USED ON ASSEMBLY
601-043-000

PLASMA SCIENCE & FUSION CENTER
MASSACHUSETTS INSTITUTE OF TECHNOLOGY

TOLERANCES UNLESS OTHERWISE SPECIFIED
DECIMALS — ANGLES ±0° 15'
3 PLACES ±.005 — 125
2 PLACES ±.010 — REMOVE ALL BURRS
1 PLACE ±0.10 — BREAK SHARP EDGES
DO NOT SCALE DRAWING

ITEM	PART NO.	DESCRIPTION	QTY.
		OUTSIDE PLATE, TYPE #2, WEDGE "D" TYPE TUNGSTEN PLATE TILE #75 - NO TAPERS	DWG SIZE C

DRAWN	SAVELLI	DATE	6 MAR 06	DWG NO.	REV
CHECKED		DATE		601-043-008	A
APPROVED		DATE			
CAD FILE:		SCALE: 4:1		SHEET: 1 OF 1	

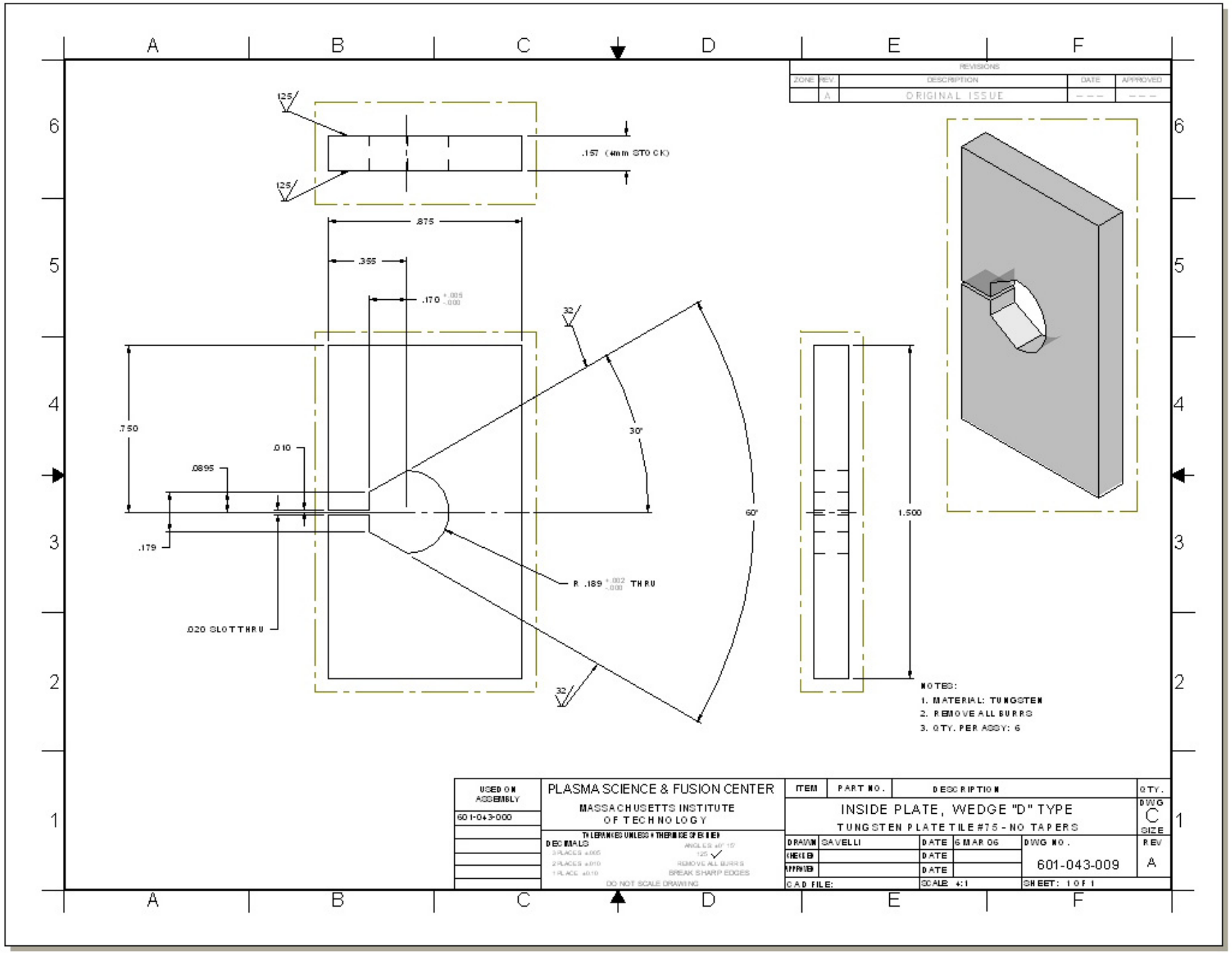
REVISIONS
ZONE REV DESCRIPTION DATE APPROVED
A ORIGINAL ISSUE
125
125
.157 (4mm STOCK)
.875
.355
.170 +.005 -.000
32
30°
60°
32
.750
.010
.0895
.179
.020 SLOT THRU
R .189 +.002 -.000 THRU
1.500
NOTES:
1. MATERIAL: TUNGSTEN
2. REMOVE ALL BURRS
3. QTY. PER ASSY: 6
USED ON ASSEMBLY
601-043-000
PLASMA SCIENCE & FUSION CENTER
MASSACHUSETTS INSTITUTE OF TECHNOLOGY
UNLESS OTHERWISE SPECIFIED
DECIMALS
3 PLACES ±.005
2 PLACES ±.010
1 PLACE ±.10
ANGLES ±0° 15'
125
REMOVE ALL BURRS
BREAK SHARP EDGES
DO NOT SCALE DRAWING
ITEM PART NO. DESCRIPTION QTY.
INSIDE PLATE, WEDGE "D" TYPE
TUNGSTEN PLATE TILE #75 - NO TAPERS
DWG C SIZE
DRAWN GAVELLI DATE 6 MAR 06
CHECKED DATE
APPROVED DATE
DWG NO. 601-043-009
REV A
CAD FILE:
SCALE 4:1
SHEET 1 OF 1

REVISIONS				
ZONE	REV	DESCRIPTION	DATE	APPROVED
	A	ORIGINAL ISSUE	---	---

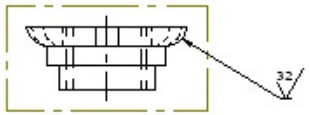

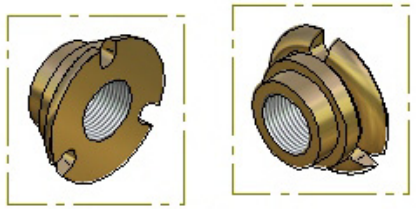

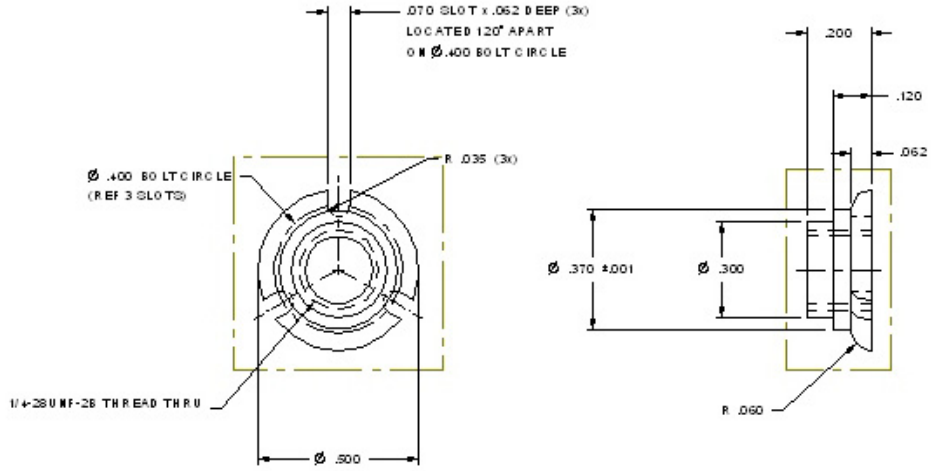

NOTES:
1. MATERIAL: TZM
2. REMOVE ALL BURRS
3. QTY. PER ASSY: 1

USED ON ASSEMBLY	PLASMA SCIENCE & FUSION CENTER	ITEM	PART NO.	DESCRIPTION	QTY.
601-043-000	MASSACHUSETTS INSTITUTE OF TECHNOLOGY			SHOULDER NUT, WEDGE "D" TYPE TUNGSTEN PLATE TILE #75 - NO TAPERS	DWG SIZE C
	TOLERANCES UNLESS OTHERWISE SPECIFIED: DECIMALS 3 PLACES ±.005, 2 PLACES ±.010, 1 PLACE ±.030; ANGLES ±0° 15'; 125; REMOVE ALL BURRS; BREAK SHARP EDGES; DO NOT SCALE DRAWING	DRAWN	GAVELLI	DATE 8 FEB 06	DWG NO. 601-043-010 REV A
		CHECKED		DATE	
		APPROVED		DATE	
		CAD FILE:		SCALE 4:1	SHEET: 1 OF 1

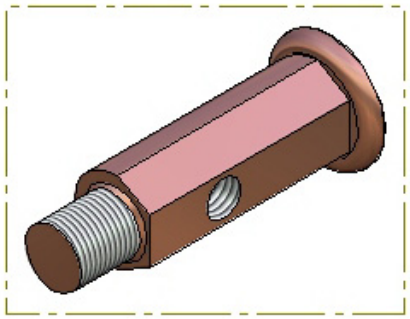

REVISIONS				
ZONE	REV.	DESCRIPTION	DATE	APPROVED
	A	ORIGINAL ISSUE	---	---
	B	.240 WAS .220, .283 WAS .258, 1.243 REF WAS 1.218 REF	4.6.06	

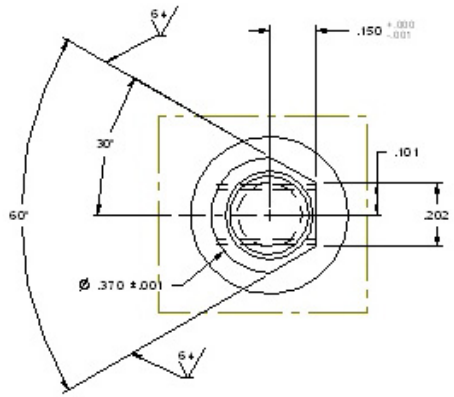

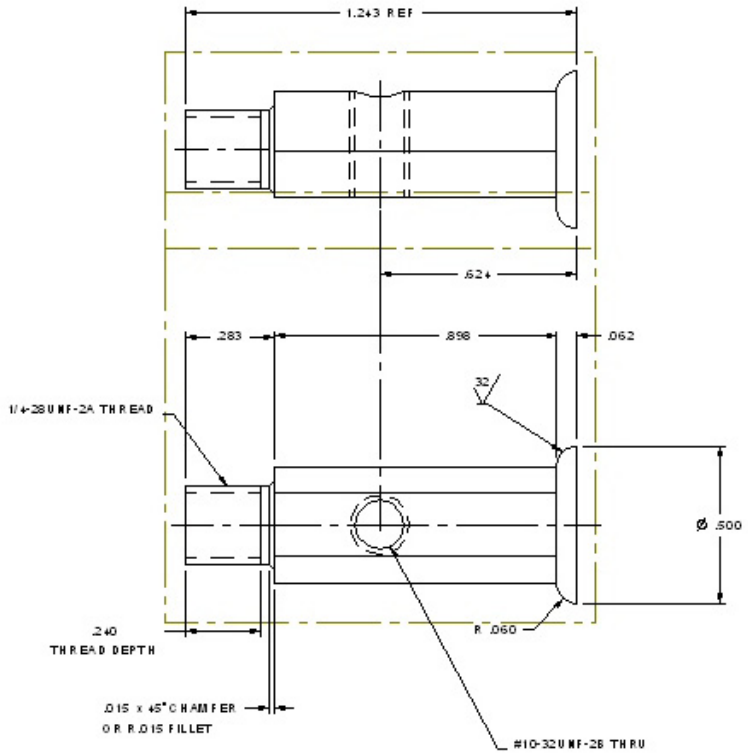

NOTES:
1. MATERIAL: TZM
2. REMOVE ALL BURRS
3. QTY. PER ASSY: 1

USED ON ASSEMBLY	PLASMA SCIENCE & FUSION CENTER	ITEM	PART NO.	DESCRIPTION	QTY.
601-043-000	MASSACHUSETTS INSTITUTE OF TECHNOLOGY			SHOULDER SCREW, WEDGE "D" TYPE TUNGSTEN PLATE TILE #75 - NO TAPERS	DWG C SIZE
	TOLERANCES UNLESS OTHERWISE SPECIFIED: DECIMALS 3 PLACES ±.005, 2 PLACES ±.010, 1 PLACE ±.010; ANGLES ±0° 15'; 125 ✓; REMOVE ALL BURRS; BREAK SHARP EDGES; DO NOT SCALE DRAWING	DRAWN	SAVELLI	DATE 6 MAR 06	DWG NO. 601-043-011 REV B
		CHECKED		DATE	
		APPROVED		DATE	
		CAD FILE:		SCALE 4:1	SHEET: 1 OF 1

Appendix B
Example Conforming Rough Surface Contact Conductance Calculation

The following thermal conductance example calculation is in accordance with the procedure outlined in Ref. [8] for conforming (flat) rough surfaces in vacuum.

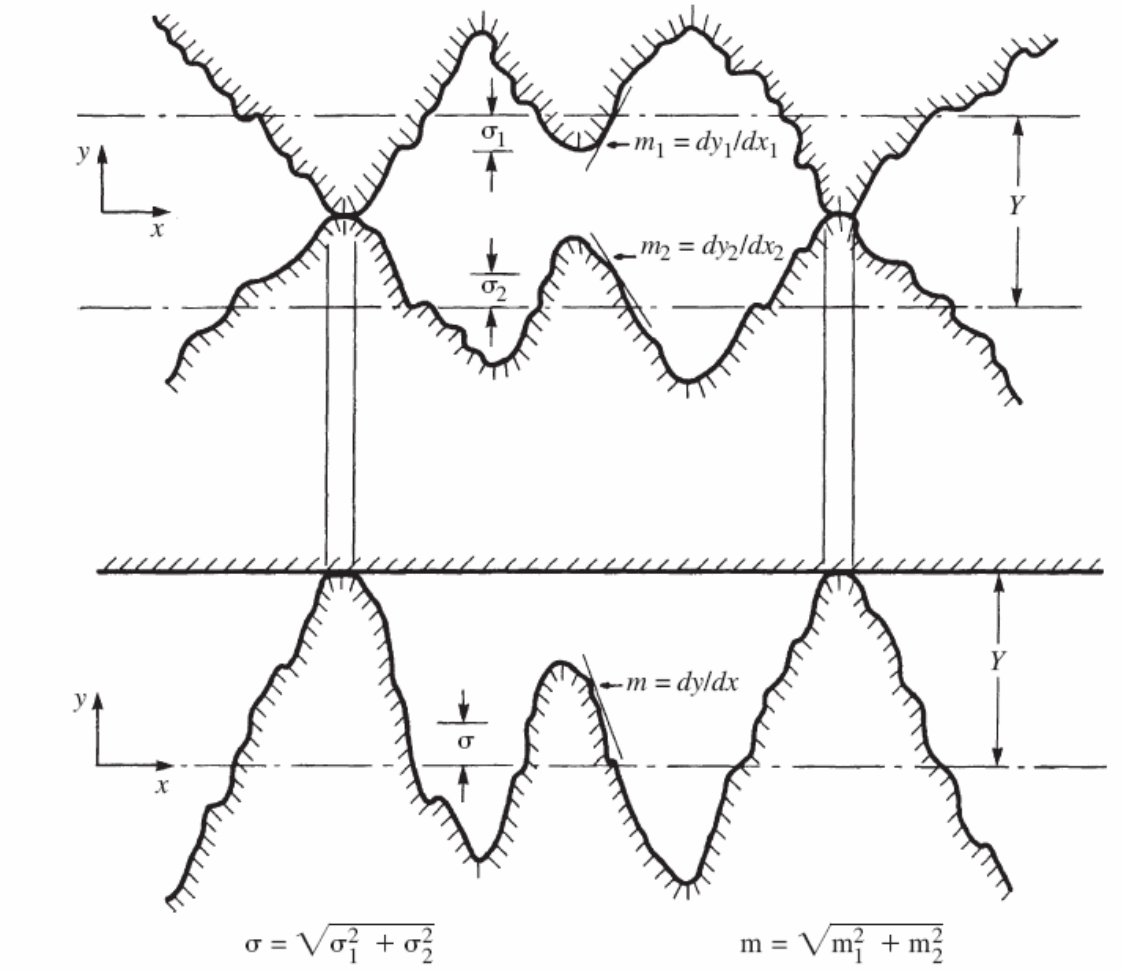

Figure 4.22 Typical joint between conforming rough surfaces. (From Hegazy, 1985.)

Function: Flatness, roughness, conductivity, hardness, pressure

W-TZM Contact Conductance

W (32RMS) - TZM (64RMS) Contact: 402 psi

Effective Thermal Conductivity - k_s

$k_1 := 163 \cdot \frac{W}{m \cdot K}$ $k_2 := 131 \cdot \frac{W}{m \cdot K}$ Thermal conductivity of materials 1 & 2

$k_s := \frac{2 \cdot k_1 \cdot k_2}{k_1 + k_2}$ $k_s = 145.259 \frac{W}{m \cdot K}$

Effective RMS Surface Roughness - σ

$\sigma_1 := .81 \cdot \mu m$ $\sigma_2 := 1.63 \cdot \mu m$ RMS surface roughness of surfaces 1 & 2

$\sigma := \sqrt{\sigma_1^{\,2} + \sigma_2^{\,2}}$ $\sigma = 1.82 \mu m$

Absolute Asperity Slopes - m_1, m_2

$\sigma_0 := 1 \cdot \mu m$

$m_1 := .076 \cdot \left(\frac{\sigma_1}{\sigma_0}\right)^{.52}$ $m_1 = 0.068$

$m_2 := .076 \cdot \left(\frac{\sigma_2}{\sigma_0}\right)^{.52}$ $m_2 = 0.098$

Effective Absolute Mean Asperity Slope - m_0

$$m_0 := \sqrt{m_1^{\,2} + m_2^{\,2}} \qquad m_0 = 0.119 \qquad \sigma_{prime} := \frac{\sigma}{\sigma_0} \qquad \sigma_{prime} = 1.82$$

Relative Contact Pressure - P/ Hp

$P := 2.77 \cdot MPa$ $H_B := 2130 \cdot MPa$ (Brinell Hardness) $H_{BGM} := 3178 \cdot MPa$

$$\kappa := \frac{H_B}{H_{BGM}} \qquad \kappa = 0.67$$

$$c_1 := H_{BGM} \cdot \left(4.0 - 5.77 \cdot \kappa + 4.0 \cdot \kappa^2 - 0.61 \cdot \kappa^3\right) \qquad c_1 = 5.549 \times 10^3\, MPa$$

$$c_2 := -0.57 + 0.82 \cdot \kappa - 0.41 \cdot \kappa^2 + .06 \cdot \kappa^3 \qquad c_2 = -0.187$$

$$P/Hp := \left[\frac{P}{c_1 \cdot \left(1.62 \cdot \frac{\sigma_{prime}}{m_0}\right)^{c_2}} \right]^{\frac{1}{1+.071 \cdot c_2}} \qquad P/Hp = 8.266 \times 10^{-4}$$

Dimensionless Contact Conductance - C_c

$C_c := 1.25P/Hp^{.95}$ $\quad C_c = 1.473\times 10^{-3}$

$h_c := \frac{C_c \cdot k_s \cdot m_0}{\sigma}$ $\quad h_c = 1.403\times 10^{4}\ \frac{W}{m^2\cdot K}$

$h_{c\_eng} := h_c$ $\quad h_{c\_eng} = 4.767\times 10^{-3}\ \frac{BTU}{s\cdot in^2\cdot R}$

Appendix C
Tile Assembly Electromagnetic Loads

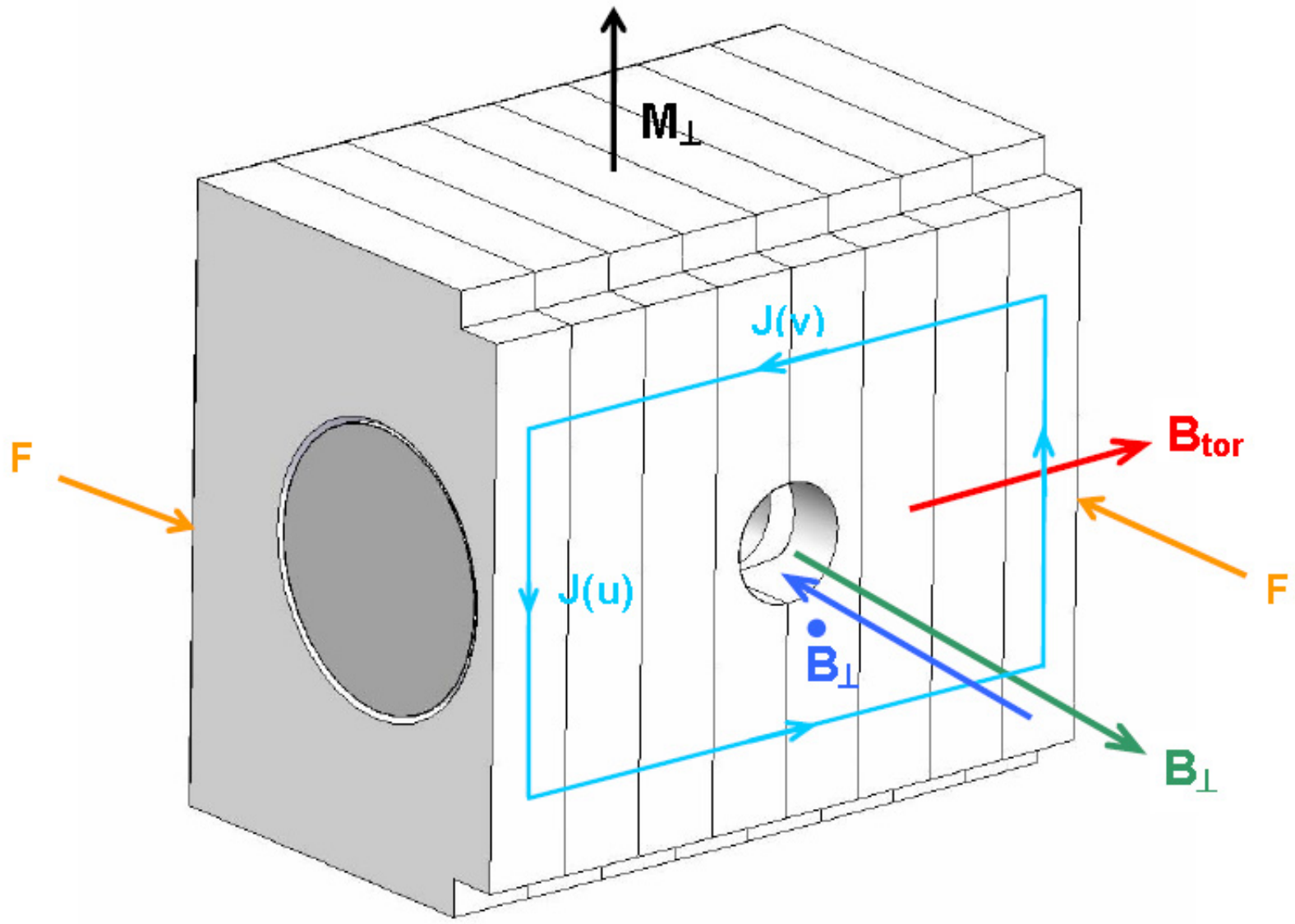

Changing Perpendicular Poloidal Magnetic Field Induced Eddy Currents and Forces

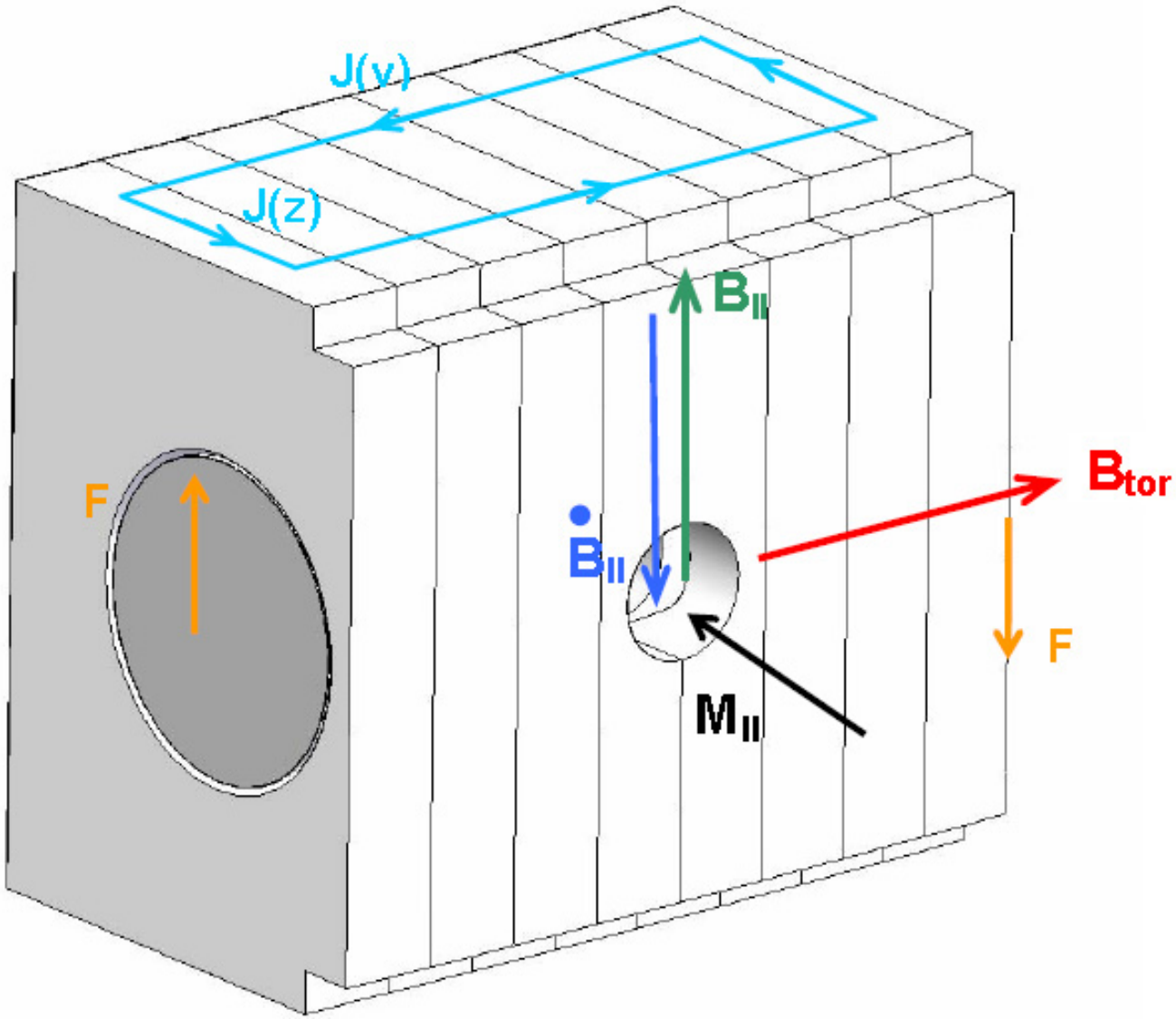

Changing Parallel Poloidal Magnetic Field Induced Eddy Currents and Forces

Tungsten Tile Calculated EMAG Rocking Moments

$H := .028 \cdot m \qquad W := .035 \cdot m \qquad D := .02 \cdot m$

$u := \frac{W}{2} \qquad u = 0.018\ m$

$v := \frac{H}{2} \qquad v = 0.014\ m$

$\alpha := \frac{H}{W} \qquad \alpha = 0.8$

$\beta := 70$

$\sigma_W := 1.85 \cdot 10^{7} \cdot \frac{1}{\Omega \cdot m}$

$B_{tor} := 7 \cdot T$

$B_{pol} := 1 \cdot T$

$t := 3 \cdot 10^{-3} \cdot s$

$dBpol/dt := \frac{B_{pol}}{t} \qquad dBpol/dt = 333.333 \frac{T}{s}$

$J(u) := \frac{-dBpol/dt \cdot \alpha^2 \cdot \sigma_W \cdot u}{\beta + \alpha^2}$

$J(u) = -9.777 \times 10^{5} \frac{A}{m^2}$

$$M_{per} := \frac{dBpol/dt \cdot B_{tor} \cdot \sigma_w}{16 \cdot (\beta + \alpha^2)} \cdot H^3 \cdot W \cdot D$$

$M_{per} = 0.587\,N \cdot m$

$M_{per} = 5.194\,in \cdot lbf$ (.56 N m, Ref. 1)

$$M_{||} := \frac{dBpol/dt \cdot B_{tor} \cdot \sigma_w}{16 \cdot (\beta + \alpha^2)} \cdot H \cdot W \cdot D^3$$

$M_{||} = 0.299\,N \cdot m$

$M_{||} = 2.65\,in \cdot lbf$

$$F_{per} := \frac{M_{per}}{W}$$

$F_{per} = 16.768\,N$

$F_{per} = 3.77\,lbf$

$$F_{||} := \frac{M_{||}}{W}$$

$F_{||} = 8.555\,N$

$F_{||} = 1.923\,lbf$

Note: These loads will be less in the actual tile assembly because of the bolt hole and the slot.

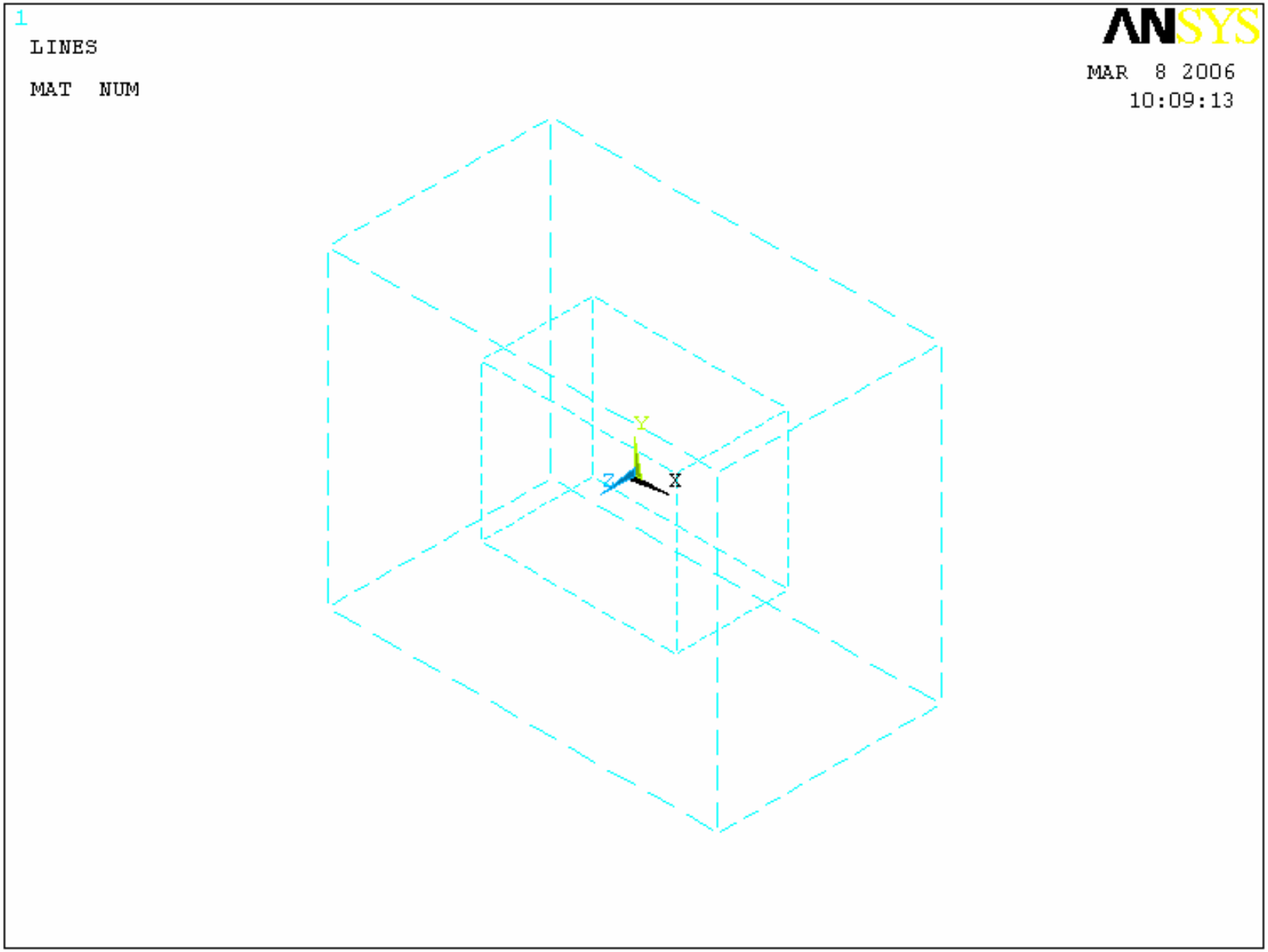

FEA EMAG Model: Air and Tungsten Volumes

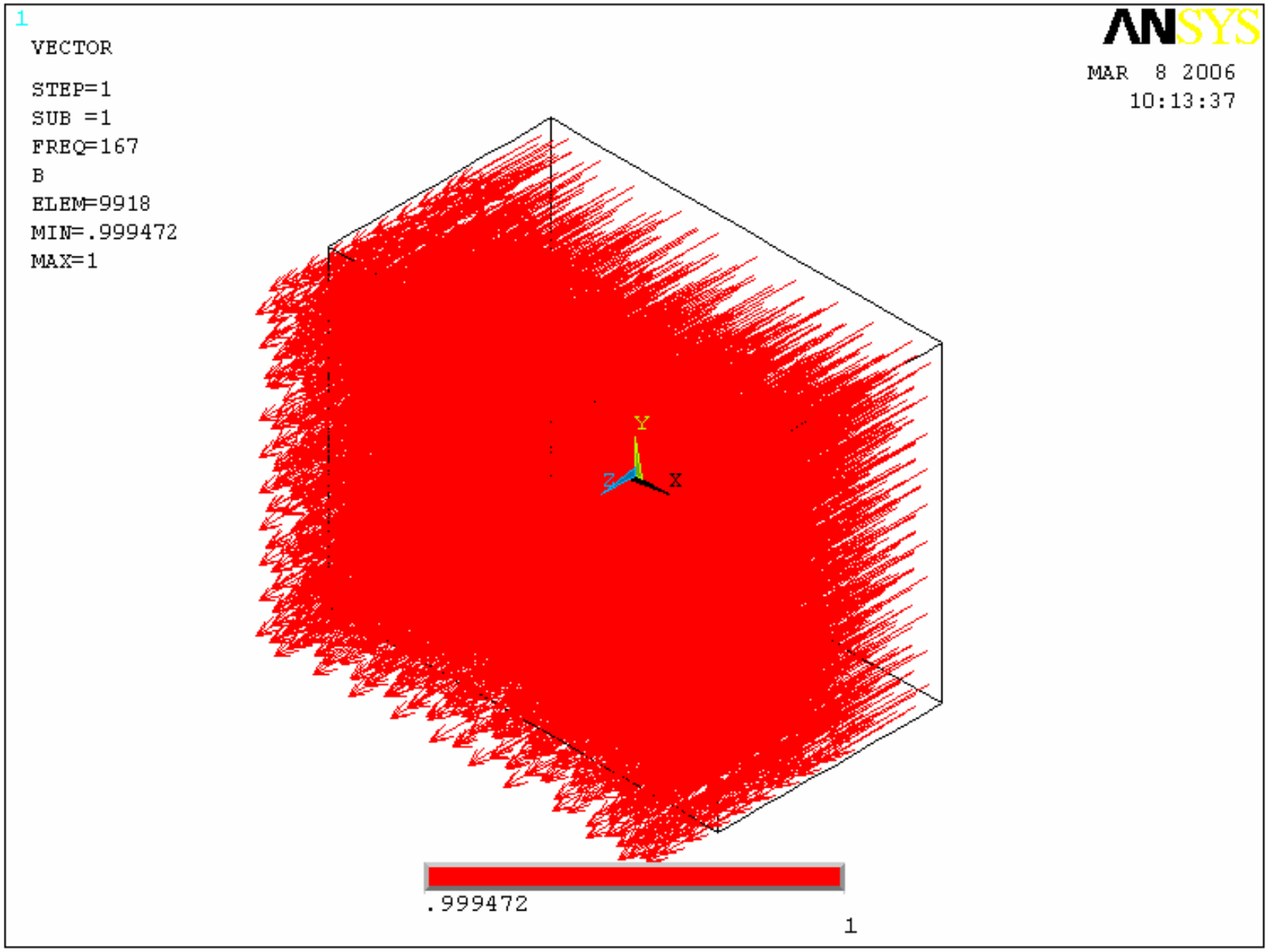

FEA EMAG Model: Poloidal Field Magnetic Flux

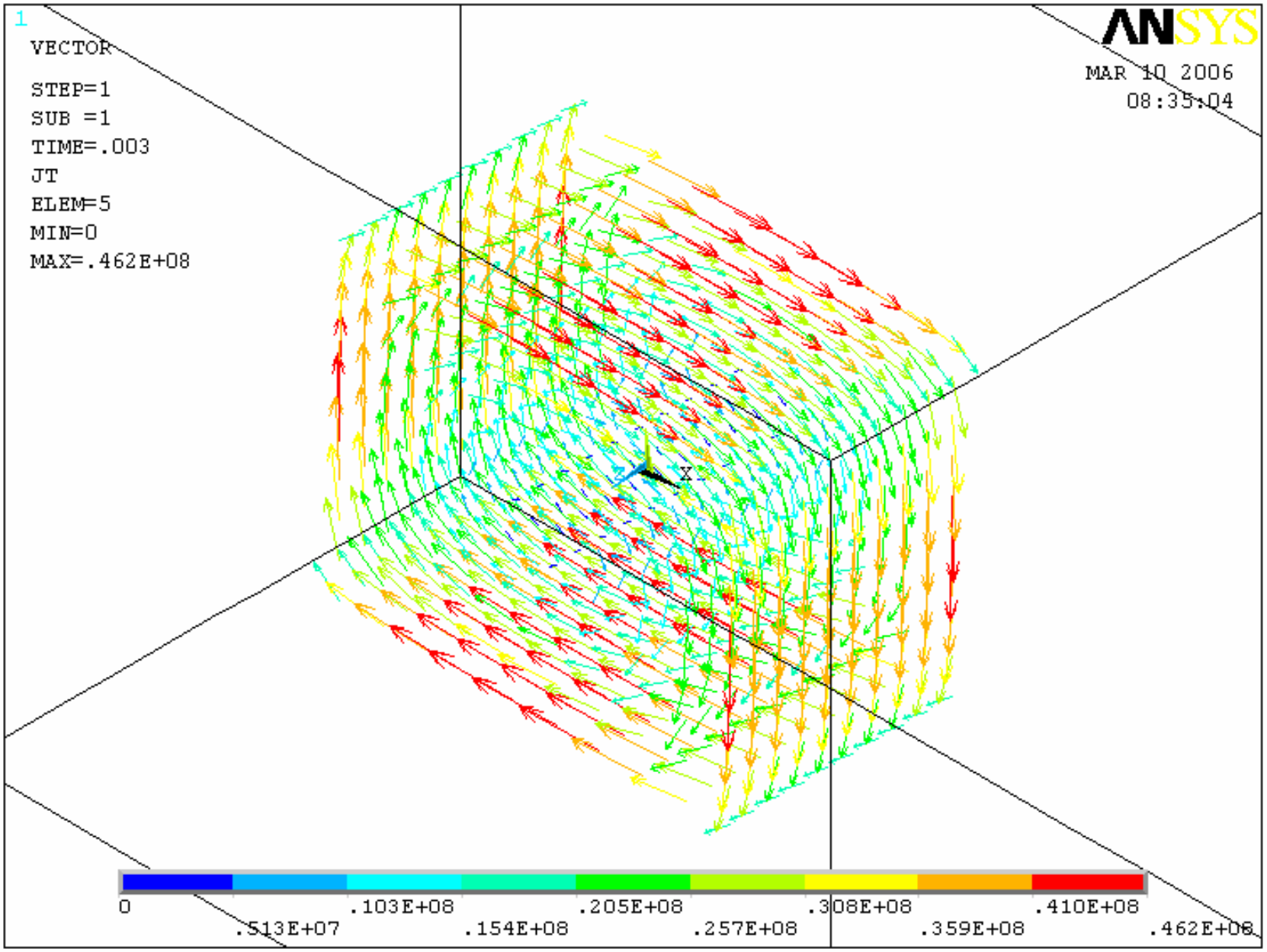

FEA Emag Model: Current Density_Beta=1 IsoView

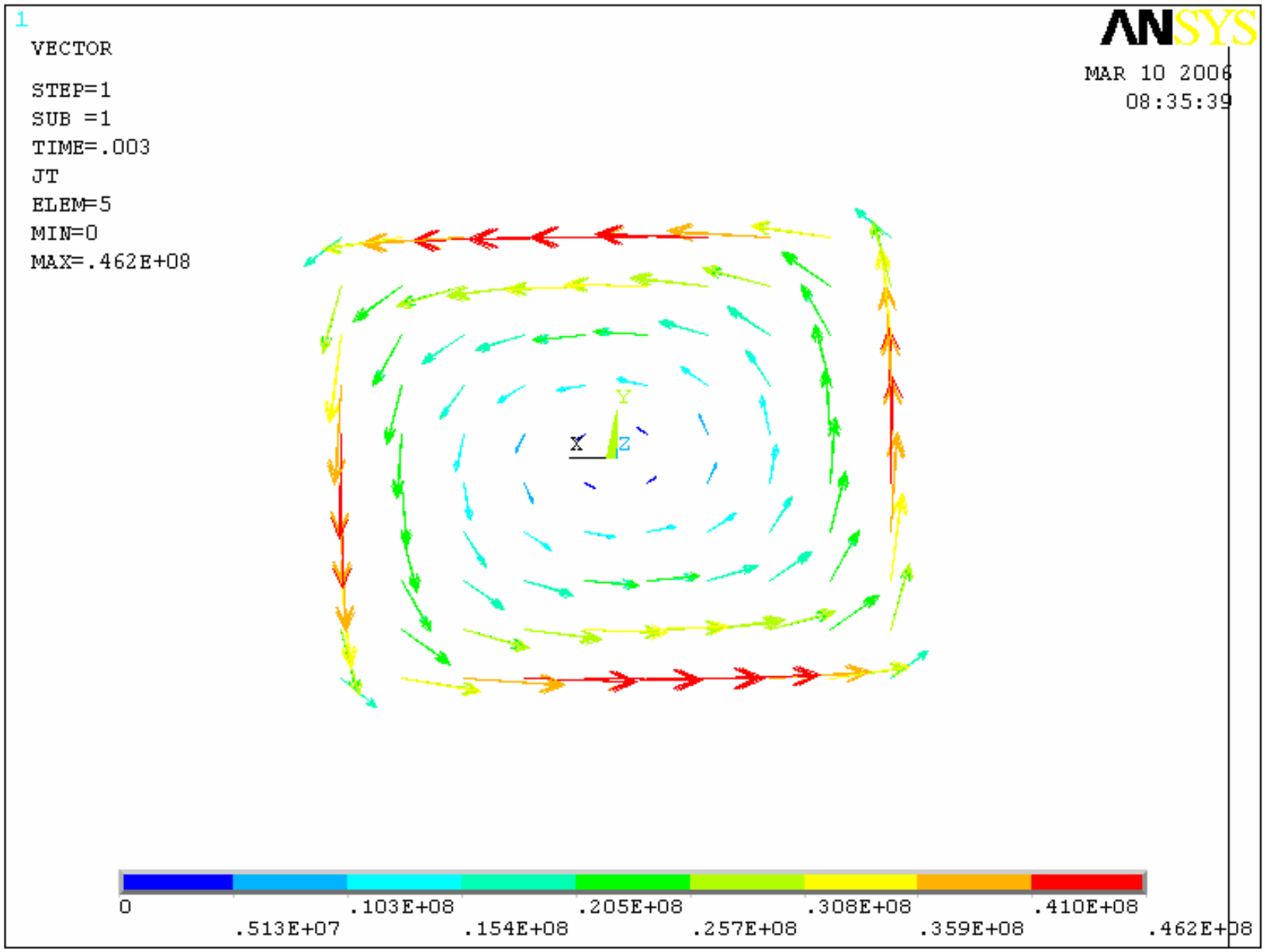

FEA EMAG Model: Current Density_Beta=1 MtgPlate View

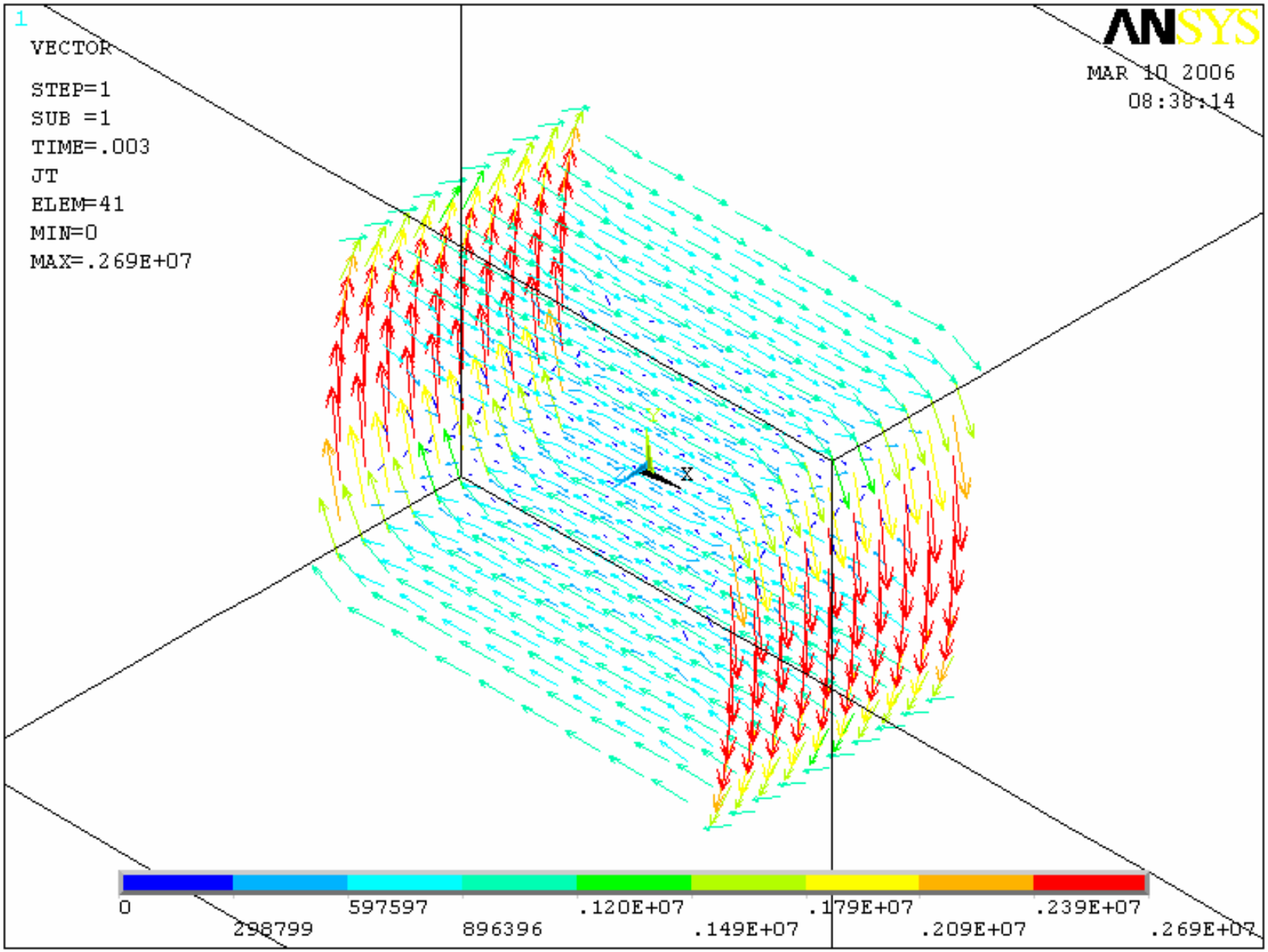

FEA EMAG Model: Current Density_Beta=70 IsoView

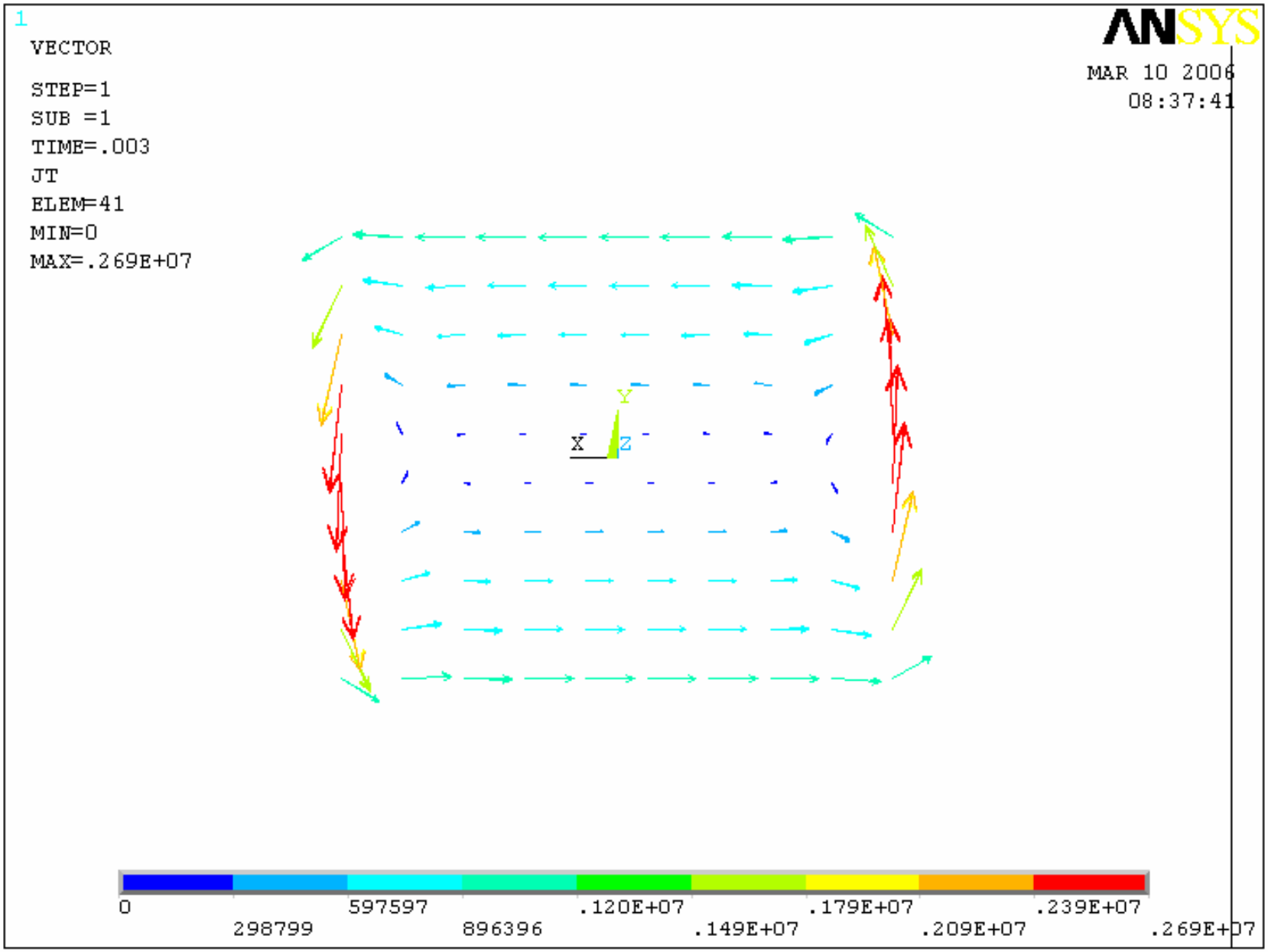

FEA EMAG Model: Current Density_Beta=70 MtgPlate View

Appendix D
Single Lamella Minimum Emag Tipping Load

Single Plate Calculated EMAG Rocking Moments

$H := .028 \cdot m \qquad W := .004 \cdot m \qquad D := .02 \cdot m$

$u := \frac{W}{2} \qquad u = 2 \times 10^{-3}\ m$

$v := \frac{H}{2} \qquad v = 0.014\ m$

$\alpha := \frac{H}{W} \qquad \alpha = 7$

$\beta := 1$

$\sigma_W := 1.85 \cdot 10^7 \cdot \frac{1}{\Omega \cdot m}$

$B_{tor} := 7 \cdot T$

$B_{pol} := 1 \cdot T$

$t := 3 \cdot 10^{-3} \cdot s$

$dBpol/dt := \frac{B_{pol}}{t} \qquad dBpol/dt = 333.333 \frac{T}{s}$

$J(u) := \frac{-dBpol/dt \cdot \alpha^2 \cdot \sigma_W \cdot u}{\beta + \alpha^2}$

$J(u) = -1.209 \times 10^7 \frac{A}{m^2}$

$$M_{per} := \frac{dBpol/dt \cdot B_{tor} \cdot \sigma_w}{16 \cdot (\beta + \alpha^2)} \cdot H^3 \cdot W \cdot D$$

$M_{per} = 0.095 N \cdot m$

$M_{per} = 0.839 in \cdot lbf$

$$M_{||} := \frac{dBpol/dt \cdot B_{tor} \cdot \sigma_w}{16 \cdot (\beta + \alpha^2)} \cdot H \cdot W \cdot D^3$$

$M_{||} = 0.048 N \cdot m$

$M_{||} = 0.428 in \cdot lbf$

$$F_{per} := \frac{M_{per}}{W}$$

$F_{per} = 23.69\ N$

$F_{per} = 5.326 lbf$ (Tipping Load)

$$F_{||} := \frac{M_{||}}{W}$$

$F_{||} = 12.087\ N$

$F_{||} = 2.717 lbf$

Note: These loads will be less in the actual plate because of the bolt hole and the slot.

09